The Quest for the Cosmological Parameters

M. Plionis[1,2]

[1] Institute of Astronomy & Astrophysics, National Observatory of Athens, 15236, Athens, Greece
[2] Instituto Nacional de Astrofisica, Optica y Electronica, Apdo. Postal 51 y 216, Puebla, Pue., C.P.72000, Mexico

Abstract. The following review is based on lectures given in the 1^{st} Samos Cosmology summer school. It presents an attempt to discuss various issues of current interest in Observational Cosmology, the selection of which as well as the emphasis given, reflects my own preference and biases. After presenting some Cosmological basics, for which I was aided by excellent text-books, I emphasize on attempts to determine some of the important cosmological parameters; the Hubble constant, the curvature and total mass content of the Universe. The outcome of these very recent studies is that the *concordance* model, that fits the majority of observations, is that with $\Omega_{\rm m} + \Omega_\Lambda = 1$, $\Omega_\Lambda \simeq 0.7$, $H_\circ \simeq 70$ km s^{-1} Mpc^{-1}, $\Omega_{\rm B} \simeq 0.04$ and spectral index of primordial fluctuations, the inflationary value $n \simeq 1$. I apologise before hand for the many important works that I have omitted and for the possible misunderstanding of those presented.

1 Background- Prerequisites

The main task of Observational Cosmology is to identify which of the idealized models, that theoretical Cosmologists construct, relates to the Universe we live in. One may think that since we cannot perform experiments and study, in a laboratory sense, the Universe as a whole, this is a futile task. Nature however has been graceful, and through the detailed and exhaustive analysis of the detected electromagnetic radiation emitted from the different photon-generating processes, we can do wonders!

Among the many important tasks of Observational Cosmology is the determination of the total mass-energy density of the Universe, the rate of its expansion, its age, the amount of ordinary and exotic matter that it contains, as well as to quantify in a objective and bias free manner the large-scale distribution of matter, as traced by galaxies, clusters of galaxies and AGN's for example.

However, these tasks are not easy to fulfil. Subjective (instrumentation, available funds, technological limitations etc) as well as objective (observational biases, limitations due to our position in space-time, etc) difficulties exist. Furthermore, we do not know whether the Universe accessible to our observations is representative of the whole Universe. A positive answer to this question is essential in order to meaningfully compare observations with theory. Under the assumption that the Universe is homogeneous and isotropic (in a statistical sense), well separated regions can be viewed as independent realizations of the same formation process. Therefore many of such regions constitute an ensemble and thus we can employ statistical techniques in our study.

In the classical Big-Bang cosmological framework the Universe indeed is considered homogeneous and isotropic on the large-scales. The most general metric satisfying this assumption, the so-called *Cosmological Principle*, is the Robertson-Walker metric (cf. [183], [35]), [112]):

$$ds^2 = c^2 dt^2 - R^2(t) \left[\frac{dr^2}{1-kr^2} + r^2(d\theta^2 + \sin^2\theta d\phi^2) \right] \quad (1)$$

where $R(t)$ is the expansion factor, k is a constant, related to curvature of space and (r, θ, ϕ) are spherical-polar coordinates. The main observational evidence that supports the choice of this model is:

- The observed expansion of the Universe. Edwin Hubble found that the redshifts of galaxies are proportional to their apparent magnitudes and assuming that they are equally luminous then their redshifts are proportional to their distances: $v \propto d$.
- The existence of the cosmic microwave background (CMB) radiation, interpreted as the relic radiation from the hot initial phase of the Universe.
- The observed light element abundances that this theory correctly predicts.

However, the observed matter distribution in the Universe is very inhomogeneous on small-scales. So, what evidence do we have supporting the validity of the Cosmological Principle?

Firstly, the *Hubble's law* is directly obtained if one assumes a homogeneous expansion of the Universe, ie., if a length χ is expanded by a factor $R(t)$, then after some time we have $d = R(t)\chi$. Differentiating we obtain the Hubble law:

$$v = \frac{\dot{R}}{R} d = H(t)\, d\,, \quad (2)$$

where $H(t)$, at the present time ($t = 0$), is the Hubble constant. Secondly, observations of distant extragalactic radio sources have shown that they are distributed across the sky in a uniform way. Other supporting evidence is provided from the decreasing - with scale - correlations of extragalactic objects and the directional independence of the correlation function. However, the most remarkable confirmation that the Universe is homogeneous and isotropic and also that it evolved from a hot dense past, was the discovery of the cosmic microwave background radiation and its high degree of isotropy across the sky. This radiation has been interpreted as the relic radiation from the time that matter decoupled from radiation, which has been freely travelling ever since. The high degree of isotropy of the CMB is direct evidence that the Universe was highly isotropic at the epoch of decoupling ($z \sim 1100$) to one part in 10^5 on scales from arc-minutes to 90°, once we subtract a local dipole anisotropy, attributed to our peculiar motion with respect to the rest-frame defined by the CMB.

1.1 Basic Elements of Dynamical Cosmology

Out of the many parameters which are essential for accurately determining the global dynamics and the formation history of the Universe; three clearly stand

out: the Hubble constant,$H_\circ$, which tells us the expansion rate of the Universe, the matter density parameter, $\Omega_{\rm m}$, which tells us how much matter, being baryonic or exotic, the Universe contains and the Cosmological constant, Λ, which tells us whether the universe is filled with an extra repulsive force. The way in which these parameters affect the cosmological evolution, are determined by the gravitational field equations and the assumed equation of state. Below, I will sketch the basic framework of standard Cosmology, in order to derive the interrelations of these parameters and how they relate to the global dynamics of the Universe.

Friedmann Equations: Within the context of a homogeneous and isotropic Universe we can derive the cosmological evolution equations using either Einstein's field equations or Newtonian gravity. The latter is possible exactly because of the Cosmological Principle, ie., we can consider any volume element, as small as necessary for Newtonian gravity to apply, as being representative of the Universe as a whole. We will derive the evolution equations for the Newtonian case, using however as an active mass density:

$$\rho^{'} = \rho + 3p/c^2 \tag{3}$$

which is given within the framework of general relativity for a homogeneous and isotropic fluid with density ρ and pressure p.

In this case we can derive the evolution equations using the mass continuity equation and Newton's equation of the motion of a small sphere. We have from the homogeneity assumption that $\nabla\rho = 0$, from isotropy that $\nabla \cdot \boldsymbol{v} = 3H(t) = 3\dot{R}/R$ and then from $\partial\rho/\partial t + \nabla \cdot (\rho\boldsymbol{v}) = 0$ we obtain:

$$\dot{\rho} + 3\left[\rho + \frac{p}{c^2}\right]\frac{\dot{R}}{R} = 0 \tag{4}$$

Rearranging (4) and using Newton's equation of motion, $\ddot{R} = -GM/R^2$, we have:

$$\frac{d}{dt}\left[\frac{1}{2}\dot{R}^2 - \frac{4\pi G}{3}\rho R^2\right] = 0 \tag{5}$$

and integrating we obtain a Newtonian analogue of cosmological evolution equation:

$$\frac{\dot{R}^2}{R^2} - \frac{8\pi G}{3}\rho = \frac{\mathcal{C}}{R^2} \tag{6}$$

where $\mathcal{C}$ is the constant of integration, which is closely related to the Newtonian energy. We can see this if we rearrange (6) as: $\dot{R}^2/2 - GM/R = -\mathcal{C}/2$. Within the relativistic formulation, the constant is in effect related to the curvature of space; $\mathcal{C} = kc^2$ and the basic equation of cosmological evolution, the *Friedmann equation*, is written:

$$\frac{\dot{R}^2}{R^2} + \frac{kc^2}{R^2} = \frac{8\pi G\rho}{3} + \frac{\Lambda c^2}{3} \tag{7}$$

where the cosmological constant (Λ) term was introduced by Einstein (rather *ad hoc*) in order to obtain his preferred static solution. Given an equation of state, $p = p(\rho)$, we can solve for ρ and then (7) can be integrated to give $R(t)$.

If we recall Newton's equation of motion, $\ddot{R} = -GM/R^2$, and we use the active density (3) and (7), we derive the second important dynamical equation of cosmological evolution. The correct relativistic form of this equation is:

$$\frac{2\ddot{R}}{R} + \frac{\dot{R}^2}{R^2} + \frac{kc^2}{R^2} = -\frac{8\pi G p}{c^2} + \Lambda c^2 \tag{8}$$

Equation of State: The question arises of which is the appropriate equation of state for the expanding Universe. The Universe expands adiabatically[1], since the symmetry imposed by the Cosmological principle implies that there is no net heat flow through any surface. Therefore as it expands, it cools (11) and since it started with a very hot phase, it will be dominated, at different epochs, by different species of particles having distinct equations of state. Relativistic particles will dominate the hot phase while non-relativistic the later cooler phases.

We can specify a unique equation of state $p = p(\rho)$ for all epochs by parameterizing it according to:

$$p = w\langle v^2 \rangle \rho \tag{9}$$

where $\langle v^2 \rangle$ is the velocity dispersion of the fluid elements. If the dominant contribution to the density comes from relativistic particles, which have $p = 1/3\rho c^2$ (when $kT \gg m_\circ v^2$, with $v^2 \simeq c^2$), then $w = 1/3$. If the dominant contribution comes from non-relativistic matter (when $kT \sim m_\circ v^2$ with $v^2 \ll c^2$) then there is negligible pressure and the dust approximation is excellent ($w = 0$).

Therefore inserting (9) into the mass continuity equation, (4), we obtain:

$$\rho \propto R^{-3(1+w)} \tag{10}$$

Armed with (10) one can now solve the Friedmann equation to get the time evolution of $R(t)$, determine the age of the Universe, etc, in the different Cosmological models.

1.2 Thermal Beginning of the Universe

The early universe, where very high densities and temperatures dominate, can be treated by using fluid thermodynamics. At very high temperatures, radiation and matter are in thermal equilibrium, coupled via Thomson scattering with the photons dominating over the nucleons ($n_\gamma/n_{\rm p} \simeq 10^9$). Therefore the primordial fluid can be treated as radiation-dominated with $p = 1/3\rho c^2 = 1/3\sigma T^4$ and from (10), we obtain:

$$T \propto R^{-1} \tag{11}$$

[1] An adiabatic process is defined as that in which there is no heat flow and thus the entropy is conserved ($\mathrm{d}S = 0$).

Therefore the temperature of the Universe drops linearly with the expansion scale factor. Furthermore, it is evident from (10), that the radiation density drops faster than the mass density and since we know from measurements that the universe is matter dominated today, then at some epoch in the past, say at a redshift $z_{\rm eq}$, we had $\rho_{\rm m} = \rho_{\rm rad}$. It is easy to show that $\rho_{\rm r} = \rho_{\rm m} R_\circ / R_{\rm eq} = (1 + z_{\rm eq})\, \rho_{\rm m}$ (the subscript $\circ$ denotes the present epoch) and using the measured values of $\rho_{\rm i}$ we have that:

$$1 + z_{\rm eq} \simeq 2.3 \times 10^4\, h^2\, \Omega_{\rm m}$$

Therefore the thermal history of the Universe can be divided in two main eras: a *radiation dominated era* ($z \gg z_{\rm eq}$) and a *matter dominated era* ($z \ll z_{\rm eq}$). In the radiation dominated era, in which we can neglect the curvature and Λ terms in Friedmann's equation (see next section), we have:

$$R \propto t^{1/2}\ .$$

By differentiating this relation with respect to time and using (7) we have:

$$t = \left(\frac{3}{32 \pi G \rho_\gamma} \right)^{1/2}\ . \tag{12}$$

Using $\rho_\gamma = \pi^2 k_{\rm b} T^4 / 15 h^3 c^5$ we finally obtain the important relation between cosmic time and the temperature of the Universe in the radiation dominated era:

$$T_{\rm Kelvin} \simeq 1.3 \times 10^{10} t_{\rm sec}^{-1/2} \tag{13}$$

from which it is evident that the Universe at early times was hot enough for nucleosynthesis to occur, as it had been supposed originally by Gamow. The era of nucleosynthesis takes place around $\sim 10^9$ K.

The Cosmic Microwave Background: Although the dynamics during the *radiation dominated era* are unaffected by ordinary matter, the electrons act as a scattering medium of the radiation and thus the Universe at this epoch is *opaque*. As the Universe cools, $\propto R^{-1}$, electrons bind electrostatically with protons to form Neutral Hydrogen. Using *Saha's ionization* equation one finds that the temperature at which the number of free electrons drops significantly is $T \simeq 3000$ K.

Therefore when the universe cools at this temperature, the scattering medium disappears and the radiation freely escapes without being absorbed or scattered which means that the Universe becomes transparent. This epoch is called the *recombination* epoch.

The existence of the relics of this radiation was predicted by Gamow and his collaborators in the 1940s. It was subsequently discovered by Penzias & Wilson in 1965, while the whole spectrum of this radiation was traced to unprecedented accuracy by the COBE satellite observations. The CMB possesses a perfect *black-body* spectrum with a mean temperature of $T_\circ = 2.728 \pm 0.004$ K and it

is extremely isotropic except for a dipole, which is however a local kinematical effect (due to our motion with respect to the cosmic rest frame defined by the CMB). From what redshift does the CMB radiation originate? From (11) we have that:

$$\frac{T}{T_\circ} = \frac{R_\circ}{R} = 1 + z$$

with $T \simeq 3000$ K and $T_\circ \simeq 2.73$ we get that

$$1 + z_{\rm rec} \simeq 1100$$

From (7) and (10) we have that in the matter dominated era $R(t) \propto t^{\frac{2}{3}}$ and thus $z_{\rm rec}$ corresponds to a time:

$$t_{\rm rec} \simeq 2.8 \times 10^{-5}\, t_\circ$$

where $t_\circ$ is the present age of the Universe. Therefore by studying the microwave background sky we have direct information from the Universe when it was as young as $t_{\rm rec}$.

The CMB dipole anisotropy: Due to our motion with respect to the isotropic CMB radiation we observe a dipole in the distribution of the radiation temperature. Although this has the appearance of a *Doppler* effect, in reality four different effects add up to produce this dipole seen by an observer moving with a velocity u. These four effects are:

- a Doppler effect that increases the frequency of photons, and thus the observed energy, seen in the direction of motion by a Doppler factor $D \equiv 1 + (u/c)\cos\theta$
- the interval of frequencies increases by the same factor in the direction of motion, and therefore since $T \propto E/\delta\nu$, the above two effects cancel out.
- the moving observer selects in the direction of motion relatively more photons by a factor D
- the solid angle in the direction of motion is smaller by a factor D^{-2} due to abberation.

The net effect is that the moving observer sees an intensity of CMB radiation $I_{\rm mov} = (1 + u/c\cos\theta)^3 I_{\rm rest}$. Due to the adiabatic expansion of the Universe, $(T \propto R^{-1})$, the shape of the Planck spectrum:

$$I_\nu = \frac{4\pi h\nu^3}{c}\left[\exp\left(\frac{h\nu}{kT}\right) - 1\right]^{-1}$$

should be preserved, which then necessarily implies that $T(\theta) = (1+u/c\ \cos\theta)T_0$ and thus:

$$\frac{\Delta T}{T} = \frac{u}{c}\cos\theta\ . \tag{14}$$

COBE observed a CMB dipole amplitude of $\delta T \sim 3.3(\pm 0.2)$ mK (which corresponds to a fluctuation $\delta T/T = 1.2(\pm 0.03) \times 10^{-3}$). The corresponding velocity of Earth is:

$$\boldsymbol{v}_{\odot} - \boldsymbol{v}_{\rm CMB} \approx 365(\pm 18) \text{ km/sec}$$

towards the galactic coordinates $(l, b) = (265^{\circ}, 48^{\circ})$ (see [159]). This motion is due to the vectorial sum of the motion of the Earth around the Sun, of the Sun within the Galaxy, of the Galaxy within the Local Group and of the peculiar motion of the Local Group, due to the gravitational effects of large-scale density fluctuations. The motion of the Earth with respect to the LG centroid is:

$$\boldsymbol{v}_{\odot} - \boldsymbol{v}_{\rm LG} \approx 308 \text{ km/sec}$$

towards $(l, b) = (107^{\circ}, -7^{\circ})$ and thus we find the velocity of the LG centroid with respect to the CMB:

$$\boldsymbol{v}_{\rm LG} - \boldsymbol{v}_{\rm CMB} \approx 620 \text{ km/sec}$$

towards $(l, b) = (277^{\circ}, 30^{\circ})$.

The Local Group velocity was originally thought as the result of the attraction of the Local Supercluster (Virgo). However, there is a residual velocity of ~ 400 km/sec that must be due to gravitational forces acting on the LG from distances greater than the Local Supercluster's centre-of-mass ($cz \sim 1100$ km/sec). Many earlier studies pointed towards the *'Great Attractor'*, a mass concentration of $\sim 5 \times 10^{16}\ M_{\odot}$ located at a distance of 42 h^{-1} Mpc and at low Galactic latitudes, as being the sole cause of a relatively local coherent motion, in which the Local Group partakes (cf. [94], [93]). Later studies, indicated that another very massive and more distant ($\sim 140\ h^{-1}$ Mpc) attractor could play a significant role in shaping the local dynamics ([151], [152], [122]). It seems that the coherence scale of the velocity field could extend to even larger distances than what originally thought (cf. [11], however for a different view see [40]).

1.3 Cosmological Parameters

Based on (7) we can define some very important parameters like the *Critical Density*, which is the density necessary to obtain a flat Universe ($\Lambda = 0$):

$$\rho_{\rm cr} = \frac{3H_{\circ}^2}{8\pi G} = 1.88 \times 10^{-29} h^2 \text{ gm cm}^{-3} \tag{15}$$

and the *Cosmological density parameter* Ω, which is a unit-less measure of the density of the Universe:

$$\Omega = \frac{\rho}{\rho_{\rm cr}} \tag{16}$$

Furthermore, the constant of proportionality in Hubble's law, the *Hubble constant*, is:

$$H_{\circ} = 100\ h\ \frac{\rm km}{\rm sec\ Mpc} = 1.023 \times 10^{-10}\ h \text{ years}^{-1} \tag{17}$$

Note that the necessity of parametrizing with h was due to earlier discordant determinations of $H_\circ$. Today most studies converge to a value of ~ 0.7 (see section 2.4).

A convenient representation of these interrelations can be produced by re-writing Friedmann's equation, in the matter dominated era (using 10), as following:

$$\frac{\dot{R}}{R} = H_\circ \left(\Omega_{\rm m}(1+z)^3 + \Omega_{\rm k}(1+z)^2 + \Omega_\Lambda\right)^{1/2} \Longrightarrow H(z) = H_\circ E(z) \qquad (18)$$

were the contribution to the total density parameter from the curvature and Λ terms is:

$$\Omega_{\rm k} = -\frac{kc^2}{H_\circ^2 R_\circ^2}\ , \qquad \Omega_\Lambda = \frac{\Lambda c^2}{3H_\circ^2}\ . \qquad (19)$$

Note that $H(z)$ is called *Hubble function*. It is evident that at the present epoch we obtain from (18) that $E(0) = 1$ and thus:

$$\Omega_{\rm m} + \Omega_{\rm k} + \Omega_\Lambda = 1 \qquad (20)$$

which also holds for any epoch (evaluated directly from 7). Note that we can have a flat Universe ($\Omega_{\rm k} = 0$) while having $\Omega_{\rm m} < 1$ (as suggested by many different observations).

The Age of the Universe: Using (18), evaluated at the present epoch, we have $\dot{R}/R_\circ = H_\circ E(z)/(1+z)$ and from ${\rm d}R/R_\circ = -{\rm d}z/(1+z)^2$ we obtain the age of the Universe:

$$t_\circ = \frac{1}{H_\circ}\int_0^\infty \frac{{\rm d}z}{(1+z)E(z)} \qquad (21)$$

For example, in an *Einstein-de Sitter* universe ($\Omega_\Lambda = \Omega_{\rm k} = 0$) we have:

$$t_\circ = \frac{2}{3H_\circ} \qquad (22)$$

while for a $\Omega_\Lambda > 0$ model we obtain:

$$t_\circ^\Lambda = \frac{2}{3H_\circ}\frac{1}{\sqrt{\Omega_\Lambda}}\sinh^{-1}\left[\sqrt{\frac{\Omega_\Lambda}{\Omega_{\rm m}}}\right] \qquad (23)$$

We therefore see that if $\Omega_\Lambda > 0$ we have that the age of the Universe is larger than what is predicted in an Einstein-de Sitter Universe.

The $\Lambda \neq 0$ Universe: Due to the recent exciting observational indications for a positive cosmological constant and the important consequences that this has to our understanding of the Cosmos, we will briefly present this model.

Originally, the cosmological Λ-parameter was introduced *ad hoc* by Einstein in his field equations in order to get a static solution ($\dot{R} = \ddot{R} = 0$). From (8)

he derived $R = (k/\Lambda_{\rm c})^{1/2}$ and inserting this into (7) he obtained, in a matter dominated ($p = 0$) Universe:

$$\rho = \frac{\Lambda_{\rm c} c^2}{4\pi G} \tag{24}$$

where $\Lambda_{\rm c}$ is the critical value of Λ for which $\dot{R} = \ddot{R} = 0$. However, it was found that his solution was unstable and that small perturbations of the value of $\Lambda_{\rm c}$ would change drastically the behaviour of R. From (7) we see that if $k \leq 0$, then $\dot{R}^2$ is always nonnegative for $\Lambda > 0$, and thus the universe expands for ever, while if $\Lambda < 0$ then the universe can expand and then recontract again (as in the $k = 1$, $\Lambda = 0$ case).

The recent SNIa observations (see section 3.2) and the CMB power-spectrum results (see section 3.1) have shown that the *Standard* Cosmological paradigm should be considered that of a flat, $\Omega_\Lambda \simeq 0.7$, $\Omega_{\rm m} \simeq 0.3$ model. Thus we will consider such a model in the following discussion. Evaluating (7) at the present epoch, changing successively variables: $x = R^{3/2}$, $y = x(\Omega_{\rm m}/\Omega_\Lambda)^{1/2}\, R_\circ^{-3/2}$ and $\theta = \sinh^{-1} y$ and then integrating, we obtain:

$$t = \frac{2}{3H_\circ\sqrt{\Omega_\Lambda}} \sinh^{-1}\left[\left(\frac{\Omega_\Lambda}{\Omega_{\rm m}}\right)^{\frac{1}{2}} \left(\frac{R}{R_\circ}\right)^{\frac{3}{2}}\right] \tag{25}$$

and

$$R = R_\circ \left(\frac{\Omega_{\rm m}}{\Omega_\Lambda}\right)^{\frac{1}{3}} \sinh^{\frac{2}{3}}\left(\frac{3H_\circ\sqrt{\Omega_\Lambda}}{2}\, t\right) \tag{26}$$

It is interesting to note that in this model there is an epoch which corresponds to a value of $R = R_{\rm I}$, where the expansion slows down and remains in a quasi-stationary phase for some time, expanding with $\ddot{R} > 0$ thereafter (see Fig.1). At the quasi-stationary epoch, called the inflection point, we have $\ddot{R} = 0$ and thus from (7) by differentiation we have:

$$R_{\rm I} = \left(\frac{\Omega_m}{2\,\Omega_\Lambda}\right)^{\frac{1}{3}} R_\circ \tag{27}$$

Now from (25) and (27) we have that the age of the universe at the inflection point is:

$$t_{\rm I} = \frac{2}{3H_\circ\sqrt{\Omega_\Lambda}} \sinh^{-1}\left(\sqrt{\frac{1}{2}}\right)\ . \tag{28}$$

The Hubble function at $t_{\rm I}$ is:

$$H(t_{\rm I}) = H_\circ\sqrt{\Omega_\Lambda}\coth\left(\frac{3H_\circ\sqrt{\Omega_\Lambda}}{2}\, t_{\rm I}\right) \Longrightarrow H_{\rm I} = H_\circ\sqrt{3\Omega_\Lambda}$$

so if $t_\circ > t_{\rm I}$ we must have $H_\circ < H_{\rm I}$.

This is an important result because it indicates that introducing an Ω_Λ-term, and if we live at a time that fulfils the condition $t_\circ > t_{\rm I}$, we can increase the age of

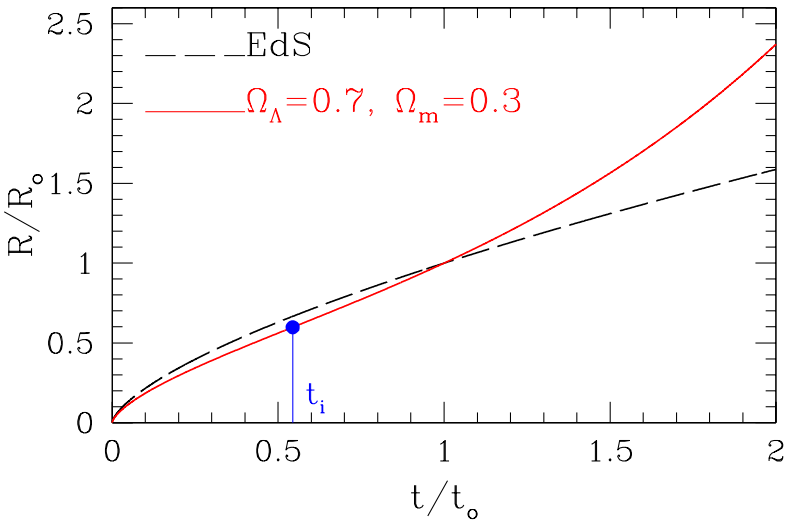

Fig. 1. The expansion of the Universe in an Einstein de-Sitter (EdS) and in the *preferred* Λ model. We indicate the inflection point beyond which the expansion accelerates. It is evident that in this model we live in the accelerated regime and thus the age of the Universe is larger than the Hubble time ($H_\circ^{-1}$).

the universe to comfortably fit the globular cluster ages while keeping the value of $\Omega_{\rm m} < 1$ and also a flat ($\Omega_{\rm k} = 0$) space geometry. From (28) and (23) and for the preferred values $\Omega_\Lambda = 0.7$ and $\Omega_{\rm m} = 0.3$ we indeed obtain $t_\circ/t_{\rm I} \simeq 1.84$ (see also Fig.1), which implies that we live in the accelerated phase of the Universe. Note that in order for the present time ($t_\circ$) to be in the accelerated phase of the expansion we must have: $\Omega_\Lambda > 1/3$.

Importance of k and Λ terms in global dynamics: Due to the recent interest in the $\Lambda > 0$, $k = 0$ Universes, it is important to investigate the dynamical effects that this term may have in the evolution of the Universe and thus also in the structure formation processes (see Fig.2). We realize these effects by inspecting the magnitudes of the two terms in the right hand side of (7). We have the density term:

$$\frac{8\pi G\rho}{3} = \frac{8\pi G\rho_\circ}{3}(1+z)^3 = H_\circ^2 \Omega_{\rm m}\,(1+z)^3$$

and from (20) we have

$$\frac{\Lambda c^2}{3} = H_\circ^2(1-\Omega_{\rm m}) \tag{29}$$

By equating the above two terms we can find the redshift at which they have equal contributions to the dynamics of the Universe. Evidently this happens only

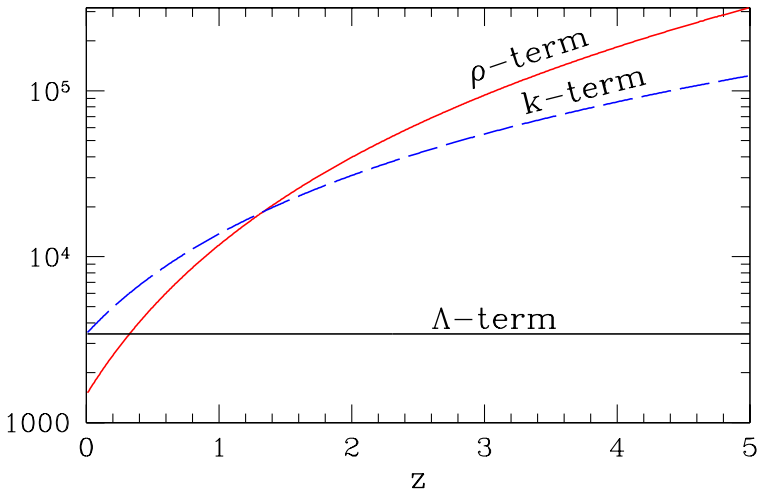

Fig. 2. The strength of the three factors shaping the recent dynamics of the Universe. Compare the strength of the ρ and Λ term ($k = 0$) and of the ρ and k term. We have assumed $H_\circ = 72$ km s^{-1} Mpc^{-1}, $\Omega_{\rm m} = 0.3$ and $\Omega_\Lambda = 0.7$.

in the very recent past:

$$z_{\rm c} = \left(\frac{\Omega_\Lambda}{\Omega_{\rm m}}\right)^{1/3} - 1 \tag{30}$$

Observations suggest that $\Omega_{\rm m} \simeq 0.3$ and $\Omega_\Lambda \simeq 0.7$, and therefore we have $z_{\rm c} \simeq 0.3$, which implies that the present dynamics of the universe are dominated by the Λ-term, although for the largest part of the history of the Universe the determining factor in shaping its dynamical evolution is the matter content. Similar results are found for the k-term in $\Lambda = 0$ models. In this case we have from (29) that

$$\frac{kc^2}{R^2} = H_\circ^2 (1+z)^2 |1 - \Omega_{\rm m}|$$

and thus the redshift at which the density and curvature terms have equal impact in the global dynamics, is:

$$z_{\rm c} = \frac{1}{\Omega_{\rm m}} - 2 \, .$$

We see that as z increases the density term grows faster than the curvature term which is important only very recently. A similar line of argument shows that also in the radiation dominated era the Λ and k terms do not affect the dynamics of the Universe.

Density parameter as a function of z: From (18) and eliminating the curvature term, using $\Omega_{\rm k} = 1 - \Omega_{\rm m} - \Omega_\Lambda$, we obtain the time evolution of the density

parameter $\Omega_{\rm m}$:

$$H^2 = H_\circ^2 \left[\Omega_{\rm m}(1+z)^3 + (1-\Omega_{\rm m}-\Omega_\Lambda)\,(1+z)^2 + \Omega_\Lambda\right] \tag{31}$$

and using (15) and (10) we have:

$$\Omega(z) = \frac{\Omega_{\rm m}}{\Omega_{\rm m} + (1-\Omega_{\rm m})(1+z)^{-1} - \Omega_\Lambda(1+z)^{-1}\left[1-1/(1+z)^2\right]} \tag{32}$$

It is easy to see that whatever the value of $\Omega_{\rm m}$, at large z we always have $\Omega(z) = 1$.

1.4 Distribution of Matter in the Universe

The task of determining and quantifying the 3-dimensional distribution of extra-galactic objects, is not a trivial. Limitations are imposed on us by our position in space-time, and also the fact that we are located in the plane of a dusty spiral galaxy, which means that the light-absorbing interstellar dust will cause the magnitudes and sizes of galaxies to decrease, especially if we observe towards the Galactic plane.

Generally in order to be able to quantify the geometry and topology of the large-scale structure of the Universe and to discriminate between the competing scenarios of structure formation, two at least issues should be addressed:
(a) The quantification, in an objective manner, of the observed structure on large scales. For this we need to observe the positions and redshifts of galaxies tracing large-volumes, large enough to be considered a fair sample of the Universe. If not we can be influenced by local *anomalies* (like a local attractor or a local underdense region) and thus the interpretation of our results could lead us to erroneous conclusions. Today there are large samples available, complete to some apparent magnitude limit which are deep enough for volume-limited samples to be extracted from them (for example the PSCZ, ORS, LAS CAMPANAS, APM, SSRS, 2dF, SDSS catalogues).
(b) The application of well defined and easily applicable statistics, which are able to distinguish between the different theoretical scenarios of structure formation and to compare between these scenarios and the observed topology and geometry of the large-scale structure of the Universe.

Of historical interest are the first attempts to quantify the distribution of galaxies by Bok and Mowbray (in the mid 1930s). They compared the variance of galaxy counts N with that expected from a Poisson distribution (ie, compared $\langle N\rangle^{1/2}$ with $\sigma \equiv [\frac{1}{M}\sum(N_{\rm i}-\langle N\rangle)^2]^{1/2}$, where M is the number of fields) and concluded that $\sigma \gg \langle N\rangle^{1/2}$ an indication that *galaxies cluster*. More sophisticated statistics appear in the mid-50's when the large Lick galaxy counting project started giving its first results (cf. [114]). Through the years a wide variety of statistical techniques have been developed in order to study the geometry and topology of the distribution of matter on large-scales (for reviews see [22] [34]).

Galaxies: Galaxies are the basic units of the distribution of matter in the universe. They are conglomerations of stars, dust and gas having typical sizes of a few kpc. Only recently, in the 1920s, was it realized that the fuzzy nebulae, that we now know to be galaxies, were not part of the Milky-Way. There appear to be many different types of galaxies, having different shapes, amounts of gas and dust, as well as star-forming regions. Many attempts have been made to produce a reliable classification scheme that bears relation to physical quantities. Galaxies come into three main categories: ellipticals, spirals and irregulars, in which the basic difference, as their names imply, is their apparent shape. However, further subdivision is essential in order to classify reliably the large variety of galaxies.

The first attempt to classify galaxies was that of Hubble in 1926. His principal morphological classification was provided by the "tuning-fork" diagram, in which the position of a galaxy was determined by the size of its nucleus and on the spiral arm tilt. For historical reasons, galaxies at the left of the diagram are called "early types" while at the right "late types". Although this diagram was produced on the basis of appearance there seem to be a link between morphology and galaxy evolution since the integrated colours and spectral types monotonically increase from left to right ([178] and references therein). The fraction of the different galaxy types is: $\sim 10\%$ ellipticals (E), $\sim 20\%$ SOs, $\sim 65\%$ spirals (S) and $\sim 5\%$ irregulars (Irr).

The spiral galaxies consist of three components: disk, bulge and halo. The disk is very thin (a few hundred pc thick). The surface brightness of stars in a typical disk falls exponentially with radius:

$$I_{\rm s} = I_{\circ} \exp\left[-r/b\right] \tag{33}$$

where b is the scale-length of the disk (typically ~ 4 kpc). The spiral structure is thought to be the result of rotating density waves which produce shocks in the gas-rich disk which leads to star formation.

The elliptical galaxies however, are ellipsoidal systems with an old population of stars and very little gas. They have a *de Vaucouleurs* luminosity distribution:

$$I_{\rm s} = I_{\rm e} \exp\left[-7.67((r/r_{\rm e})^{0.25} - 1)\right] \tag{34}$$

where $r_{\rm e}$ is the *effective* radius enclosing half of the total light. Therefore $I(r)$ falls off more slowly than r^{-2} for $r < r_{\rm e}$ and more rapidly for $r > r_{\rm e}$ (this formula also fits the bulges of SOs and spirals). The mass of elliptical galaxies can vary widely; from dwarfs with $M \sim 10^7\ M_{\odot}$ to supergiants with $M \sim 10^{12}\ M_{\odot}$

Groups & Clusters of Galaxies: Galaxy clusters occupy a special position in the hierarchy of cosmic structures in many respects. Being the largest bound structures in the universe, they contain hundreds of galaxies, large amounts of Dark Matter (DM) and hot X-ray emitting gas, and thus can be detected at large redshifts. Therefore, they appear to be ideal tools for studying large-scale structure, testing theories of structure formation and extracting invaluable cosmological information (see recent reviews [24], [5]) Groups of galaxies are typically systems that contain $\lesssim 10 - 20$ galaxies (for a recent review see [105]).

There are several classification schemes for clusters. A simple and clear-cut one is between *regular* and *irregular* clusters.

- ⊗ **Regulars:** They have smooth and symmetric structure, with high central density ($\geq 10^3/\mathrm{Mpc}^3$), a small fraction of spiral galaxies ($\lesssim 20\%$), high velocity dispersion ($\sim 10^3$ km/sec) and high X-ray luminosity. The high velocity dispersion as well as the smooth structure is considered to be evidence that these clusters are in virial equilibrium (relaxed). About 50% of all clusters are regulars.
- ⊗ **Irregulars:** They have lumpy structure with evident substructures, lower velocity dispersion and lower X-ray luminosity. The fraction of spirals is higher than that in regular clusters ($\gtrsim 40\%$).

Another distinct class of clusters is those having a central very bright galaxy (BCG or cD's). The BCG galaxies are giant ellipticals, some with multiple nuclei (cD's) and masses $M \gtrsim 10^{12}\ M_\odot$. There are different views regarding their formation history; one advocates that they form by "galactic cannibalism" where dynamical friction causes cluster galaxies to spiral towards the cluster core and then strong tidal effects take place (cf. [101], [9]), the other advocates that they form at *special* locations, which are the kernels around which clusters will eventually form by anisotropic accretion of matter (cf. [184] and references therein). Furthermore:

- ⧫ There is a well defined relationship between galaxy density and fraction of Hubble types. The fraction of E's and SO's increases smoothly with increasing galaxy-density ([48]). An interesting question is whether the above relation is a direct result of the galaxy formation processes, or an evolutionary effect.
- ⧫ Clusters are highly flattened systems even more than elliptical galaxies. This fact is not due to rotation (cf. [49], [141]), and therefore it either reflects the initial conditions of their formation and/or the tidal effects acting between proto-clusters. In fact, the high peaks of an initial Gaussian density field, the possible sites of cluster formation, are non-spherical ([8]). The cluster mean projected ellipticity is $\varepsilon \sim 0.5$ and there is evidence that clusters are more prolate-like (cf. [12]).
- ⧫ Neighbouring clusters tend to point to each other up to distances of $\sim 20-30$ h^{-1} Mpc (cf. [15]). Dynamically young (irregular) clusters show a tendency to be more aligned with their neighbours and are preferentially found in high-density environments ([125], [157]).

For large-scale clustering, dynamical and cosmographical studies, it is extremely important to compile large, whole-sky catalogues of groups and clusters. One of the first and extensively studied such catalogue is the ABELL/ACO catalogue [1], which was based on an eyeball selection procedure from sky survey plates. This all-sky sample contains 4073 rich clusters, nominally complete to a redshift $z = 0.2$. Its obvious limitations, due to the eyeball selection procedure, were superseded by the objectively selected APM clusters ([42]) which were based

on the APM galaxy catalogue containing 4×10^6 galaxies ([96]). This cluster catalogue covers latitudes $b < -35^\circ$ and contains 950 clusters, typically poorer than the ABELL/ACO one's. Furthermore, with the ROSAT whole-sky X-ray survey it was possible to construct X-ray selected cluster catalogues (cf. [51]), which suffer less from projection effects, which can produce *phantom* clusters. For example the REFLEX X-ray cluster sample contains ~ 450 clusters ([21]).

Fig. 3. (Included separately as a JPG image) An example of a filamentary supercluster: The 2D distribution of APM clusters members. The inserted plots show the smooth 2D galaxy density map of some of the cluster members. For the case of A3128 we overlay the X-ray emission contour plots. The cluster's elongation along the filamentary supercluster is evident.

Superclusters, Filaments & Voids: Superclusters are aggregates of clusters, groups and galaxies. They are the largest, isolated, but dynamically un-relaxed due to their size, objects in the large scale distribution of matter and thus they are ideal probes of the initial conditions that gave rise to them. This fact is because typical peculiar velocities of clusters are $v_{\rm pec} \sim 10^3$ km/sec and therefore in a Hubble time $(1/H_\circ)$ they can move no more than $\sim 10\ h^{-1}$ Mpc, which is substantially smaller than the scale of a typical supercluster. Superclusters can be identified in 3-D catalogues of clusters but also in 2-D projections of galaxy distributions. Regions of high density in clusters can be identified also on the APM galaxy map.

The large scale clustering pattern of galaxies is expected to be characterized by a filamentary and sheet-like distribution (cf. [194], [55], [179]). Indeed many authors have been finding that the vast majority of the superclusters are flattened with a predominance of filament-like shapes (cf. [13] and references therein). Figure 3 shows the 2-dimensional projection of a filamentary supercluster containing 5 APM clusters.

Superclusters are not centrally condensed objects (like clusters) and their typical size is $\sim 30 - 50\ h^{-1}$ Mpc. However larger structures, with a length $\sim 200\ h^{-1}$ Mpc, may exist (cf. [176] and references therein). Detailed studies have shown that elongated bridges ($\sim 30\ h^{-1}$ Mpc) of galaxies have been found to connect rich clusters. Since wide-angle three-dimensional surveys became available, the filamentary distribution of galaxies has been a constantly observed feature. Even the original CFA survey (cf. [72]) showed networks of filaments mostly connecting rich clusters of galaxies and large voids (cf. [116]), a fact which has been confirmed by all the recent surveys (SSRS, ORS, PSCZ etc). Voids are regions of density well below the average value. In all deep radial-velocity surveys, the velocity distribution shows striking empty regions were no (or very few) galaxies exist. It is an extremely difficult task to identify voids in 2-D projections of galaxy distributions since the projection will tend to smooth-out any such structure. An extremely interesting question, relevant to theories

of structure formation, is whether the voids are empty of luminous matter or empty of all matter.

2 Distance Scale, Hubble Constant & the Age of the Universe

One of the most important parameters in determining the fate of the Universe as a whole, is the present day expansion rate of the Universe, which is encapsulated in the value of the Hubble constant $H_\circ$. Its value sets the age of the Universe and specifies the value of the critical density $\rho_{\rm cr}$, and through this route the geometry of the Universe.

From the Hubble law (2) it is evident that in order to determine its value we need to determine the expansion velocity (redshift) as well as the distance of extragalactic objects, but within a redshift such that space-curvature effects do not affect distances (43). A further concern is that local gravitational effects produce *peculiar* velocities, that are superimposed on the general expansion. This can easily be seen in the toy model of (2), if we allow $\chi \equiv \chi(t)$. Then

$$v = H_\circ d + R\dot{\chi} \, ,$$

with the factor on the right being the peculiar velocity. Since the observer as well as the extragalactic object, of which the distance we want to measure, have peculiar velocities then the above equation becomes:

$$cz = H_\circ d + (\boldsymbol{v}(d) - \boldsymbol{v}(0)) \cdot \hat{r} \tag{35}$$

where $v(0)$ is the velocity of the observer and $\hat{r}$ is the unit vector along the line-of-sight to the extragalactic object. It is then obvious that in order to measure $H_\circ$, the local velocity field should be measured and the extragalactic distances corrected accordingly. It is easily seen that if both observer and galaxy take part in a coherent bulk flow, having the same amplitude at the observer and galaxy positions, then the right-hand part of (35) vanishes. In general however, one needs good knowledge of the velocity field in order to correct distances adequately.

2.1 Distances of Extragalactic Objects

Our only means of obtaining information and therefore knowledge of the structure and dynamics of the Universe (on all different scales) are through the electromagnetic radiation that we receive. Therefore it is of primary importance to define a system of measuring luminosities taking also into account that the Universe expands and that light loses energy through a variety of processes.

If we assume that light propagates with no loss of energy, then the apparent luminosity of a source l, is related to its absolute luminosity L, by:

$$l = \frac{L}{4\pi r^2} \tag{36}$$

where r is the distance to the source. We can see the extreme importance of determining the pair (l, L), since such knowledge would provide the distance of the source, r.

Due to historical mostly reasons we use a logarithmic brightness system by which an object with a magnitude of 1 is 100 times brighter than an object with a magnitude 6. We have:

$$m = -2.5 \log_{10} l + c_1 \qquad M = -2.5 \log_{10} L + c_2 \tag{37}$$

where m is the apparent magnitude and M the absolute one. Therefore, using (36) we have:

$$m - M = 5 \log_{10} r + c_3 \tag{38}$$

where $c_{1,2}$ are constants which depend on the filter used and c_3 is that value for which $m = M$ at a distance of 10 parsecs (see section 2.3) from the Earth, and thus $c_3 = -5$. In extragalactic astronomy, instead of pc, we use Mpc and therefore (38) becomes:

$$m - M = 5 \log_{10} r + 25 \tag{39}$$

The above definitions are somewhat *ideal*, since in the real world we do not observe the total apparent magnitude, but that corresponding to the particular range of spectral frequencies, that our detector is sensitive to, and those allowed to pass through Earth's atmosphere. If we detect l_ν over a range of frequencies $(\nu \pm \delta\nu)$, then the observed apparent magnitude is $m = -2.5 \log_{10} \int_{\delta\nu} l_\nu \mathrm{d}\nu + c$. However, neither the atmosphere nor the detectors have a sharp ν limit and therefore it is better to model these effects by a sensitivity mask F_ν, and the observed apparent magnitude is then:

$$m_{\mathrm{F}_\nu} = -2.5 \log_{10} \left[\int_0^\infty F_\nu l_\nu \mathrm{d}\nu \right] + c \tag{40}$$

If $F_\nu = 1$ then the apparent (or absolute) magnitude of a source is called the *bolometric* magnitude.

How do the above definitions change by taking into account the fact that the Universe expands? To answer this we need a metric of space-time, which in our case is the *Robertson-Walker* metric. Since light travels along null-geodesics, a fundamental concept of distance can be defined by the corresponding light-travel time, which is called *proper distance*. If a light signal is emitted at a galaxy $\mathcal{G}_1$ from the coordinate position (r_1, θ_0, ϕ_0) at time $t = 0$ and received by an observer at $\mathcal{G}_0$ at (r_0, θ_0, ϕ_0), then these events are connected only by the light signal and since all observers must measure the same speed of light, it defines a very fundamental concept of distance. Obviously, it depends on the curvature of space, and since $\mathrm{d}s = 0$ we have from (1):

$$d_{\mathrm{pro}}(t) = R(t) \int_0^{r_1} \frac{dr}{\sqrt{1 - kr^2}} = \left\{ \begin{array}{ll} R(t)\ \sin^{-1} r_1 & k = +1 \\ R(t)\ r_1 & k = 0 \\ R(t)\ \sinh^{-1} r_1 & k = -1 \end{array} \right\} \tag{41}$$

In the expanding Universe framework, the expressions (36) and (38) change, to:

$$l = \frac{L}{4\pi\ d_{\mathrm{pro}}^2 (1+z)^2}\ , \qquad m - M = 5 \log_{10} d_{\mathrm{L}} + 25 \tag{42}$$

where $d_{\rm L} \equiv d_{\rm pro}(1+z)$ is the *luminosity distance*. It is obvious that the distance measure of an extragalactic object depends on the underlying Cosmology. A proper derivation of the luminosity distance (cf. [183], [112]) provides the following expression:

$$d_{\rm L} = \frac{2c}{H_{\circ}\Omega^2}\left[\Omega z + (\Omega - 2)\left(\sqrt{1+z\Omega} - 1\right)\right] \tag{43}$$

where Ω contains all the contributions (mass, energy density, curvature).

Another important distance definition is that of the angular-diameter. It is based on the fact that a length l, subtends a smaller angle, θ, the further away it is ($l \propto 1/\theta$) and it is given from: relation to:

$$d_{\theta} = \frac{d_{\rm L}}{(1+z)^2} \tag{44}$$

Note that this notion of distance is used to derive the CMB power spectrum predictions of the different cosmological models (see section 3.1).

2.2 Biases affecting Distance Determinations

Many effects, related either to our position in space (being on the plane of a dust-rich spiral galaxy), to natural limitations (introduced for example by the expansion of the Universe) or to detector related issues, introduce systematic biases that affect our ability to measure accurately distances. Below, I list a few of the most important such effects.

K-correction: Since bolometric magnitudes are not possible to measure, but rather magnitudes over a particular wavelength range, it is important to correct these magnitudes for the effect of the expansion of the Universe. These considerations result in modifying the distance modulus by a factor, the so-called $K-$correction factor:

$$m - M = 5\log_{10} d_{\rm L} + 25 + K(z) \tag{45}$$

This factor arises from the fact that when we measure the magnitude of sources at large distances and at a particular frequency, say $\nu_{\rm o}$, we receive light emitted from a different part of the spectrum, $\nu_{\rm e}$. It could well be that in this latter part of the spectrum the extragalactic object is particularly fainter or brighter than in the nominal one, $\nu_{\rm o}$. Furthermore, a combination of different factors; evolution, intervening absorption processes or detector sensitivity for example, result in energy losses as a function of wavelength, which can be expressed by a mask $F(\nu_{\rm o})$ (40). Knowing $F(\nu_{\rm o})$ one can estimate the K-factor by integrating the spectrum at the source rest frame. For example, such calculations have shown that a typical value for spiral galaxies at $z = 1$ is $K \approx 2$ (in general $K(z) \propto z$).

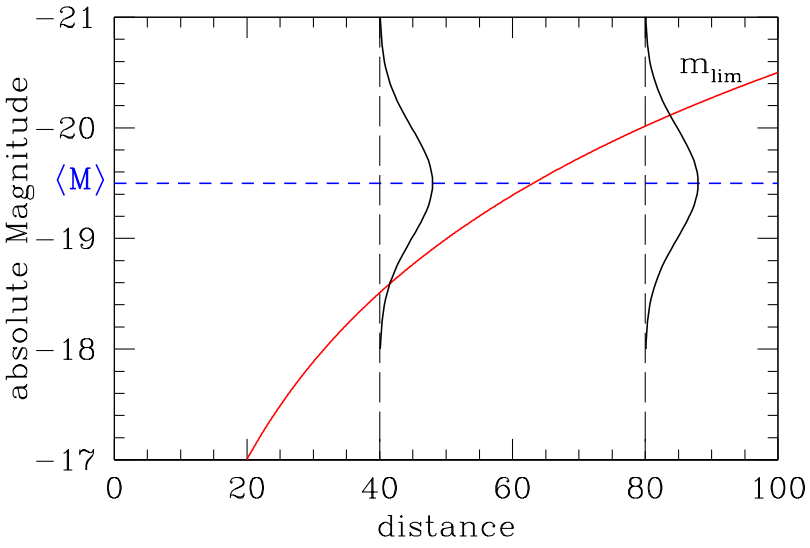

Fig. 4. Illustration of Malmquist bias: Only objects with M above the $m_{\rm lim}$ limit can be observed. At different distances different portions of the distribution around $\langle M\rangle$ can be observed.

Malmquist bias: Due to the nature of astronomical observation there is a minimum flux density above which we select extragalactic objects. As we look deeper in the Universe we tend to pick up a relatively larger fraction of intrinsically bright objects (ie., only the brighter end of the luminosity function is sampled). This bias arises when determining distances from apparent magnitude limited samples. If the individual absolute magnitudes $M_{\rm i}$ of a sample of extragalactic objects have a Gaussian distribution around $\langle M\rangle$ with dispersion σ, then this bias, for the case where the distribution of extragalactic objects is considered homogeneous, is given by:

$$\Delta(M) = 1.382\sigma^2 \tag{46}$$

How does this bias affect the determination of extragalactic distances? The inferred distances of extragalactic objects are typically smaller than their true distances. From (39) we have that:

$$r_{\rm cor} \approx r_{\rm raw}\ 10^{1.382\sigma^2/5}$$

We illustrate this bias in Fig.4; as the distance increases, $M(m_{\rm lim})$ becomes brighter and therefore the brighter end of the luminosity function is sampled. For a larger $m_{\rm lim}$ (deeper sample) the value of $M(m_{\rm lim})$ increases (less luminous) so we have a smaller $\Delta(M)$. Conversely, for a given $m_{\rm lim}$ and $\langle M\rangle$, the bias increases with distance.

Note that we have considered a fairly straight-forward case, ie. that of a sample with a unique $\langle M \rangle$ value. In real samples of extragalactic objects we have a range of such values and therefore this bias is not easily seen.

A related bias that also affects extragalactic distance determinations is the fact that there are larger numbers of objects at larger distances and therefore within a given range of estimated distances, more will be scattered by errors from larger to smaller distances than from smaller to larger ones.

Galactic absorption: Interstellar gas and dust absorbs the background light with dust scattering more efficiently the blue light, and thus the background light appears artificially reddened. From simple geometrical considerations it is easy to show that the flux l_ν of an extragalactic source, transversing a Galactic layer of thickness $\mathrm{d}s$, at an angle b from the equatorial plane, suffers losses $\delta l_\nu / l_\nu \propto \mathrm{d}s\ \mathrm{cosec}(b)$ and therefore:

$$\frac{\mathrm{d}l_\nu}{\mathrm{d}s} = -\kappa_\nu l_\nu \mathrm{cosec}(b) \tag{47}$$

where the constant of proportionality κ_ν is the absorption coefficient at the spectral frequency ν. Therefore, integrating we have:

$$l_\nu = l_\nu^o\ \exp\left[-\mathcal{A}\ \mathrm{cosec}|b|\right] \tag{48}$$

where the integration constant l_ν^o is the incident and l_ν is the observed flux, while $\mathcal{A} = \int \kappa_\nu \mathrm{d}s$ is the *optical thickness*. Therefore to take into account this effect (36) should change to:

$$l_{\mathrm{true}} = \frac{l_{\mathrm{raw}}}{\exp\left[-\mathcal{A}\mathrm{cosec}|b|\right]} = \left(\frac{L}{4\pi r^2}\right)\ \exp\left[\mathcal{A}\ \mathrm{cosec}|b|\right]\ . \tag{49}$$

Values of $\mathcal{A}$ slightly vary for different spectral frequency bands, but a generally accepted value, in V, is ~ 0.2. We see from (49) and (39) that

$$r_{\mathrm{true}} \approx r_{\mathrm{raw}} \exp\left[-\mathcal{A}\ \mathrm{cosec}|b|/2\right] \tag{50}$$

ie., the distance of an extragalactic source at a given absolute magnitude can be significantly overestimated at low galactic latitudes if this effect is not taken into account. Note however that the $\mathrm{cosec}(b)$ model is oversimplified since the distribution of gas and dust in the Galaxy is rather patchy.

Cosmological Evolution: As we look back in time we see a distribution of extragalactic objects (normal galaxies, AGN's, clusters) in different evolutionary stages. It may well be that their luminosity and/or mean number density is a function of cosmic time, a fact that will affect distance determinations based on local calibrations of the relevant scaling-relations.

Aperture effect: Since galaxies are extended objects with no sharp outer boundaries, their photometric measures will depend also on the size of the telescope aperture since at different distances different fraction of a galaxy will fit in the aperture. This is a distance–dependent effect, since diameters scale like $1/r$, and therefore it may affect the distance estimate.

2.3 Distance Indicators:

In order to develop the distance ladder from local to distant cosmic objects, one starts from the local distance scale (for a detailed account see [143] [144]).

Galactic Distance Indicators: The primary method used to estimate the distances to nearby stars is that of *Trigonometric Parallax*. As the Earth orbits the Sun, we view the Universe from different points of the orbit throughout the year. This difference is maximum every 6 months when the Earth is on the opposite side of its orbit around the Sun. This kinematic method provides the basic unit of distance, the *parsec*, used by astronomers. It is defined as the distance at which a star would have a trigonometric parallax of $1^{''}$ (parsec = *par*allax + *sec*ond):

$$1pc = 3.086 \times 10^{13} \text{ km } = 3.26 \text{ light years}$$

Note that this method is effective out to ~ 60 parsecs and that the nearest star to us (α-Centauri) is at a distance of 0.75 parsecs.

Among the many distance indicators, used to determine distances within our Galaxy, a particularly interesting one is the *Main sequence fitting* method. This takes advantage of the fact that stars in globular clusters are at a common distance and that there is a unique correlation between spectral stellar type and absolute luminosity (the *H-R* diagram). Therefore by measuring the distance, via a kinematic method, to one relatively near globular cluster, one sets the zero-point of this method and then by observing the apparent magnitude - spectral type distribution of other globular clusters, one can determine their distance.

Extragalactic Distance Indicators: The next step is based on *Cepheid Variable Stars*. This method has been traditionally used within our Galaxy and in the nearby Large Magellanic Cloud (LMC), but with the *Hubble Space Telescope* it has been successfully used out to ~ 20 Mpc (cf. [61]). A strong and tight relationship exists between the intrinsic luminosity of these stars and their period of variation (pulsation) which results in a Period-Luminosity relation:

$$L \propto \log P^{1.3} \Longrightarrow \log L = \text{zero-point} + 1.3 \log P \tag{51}$$

Once this relation has been calibrated, it provides the absolute luminosity of the distant Cepheid stars and via (39), the distance of their host galaxy. Although this relation has a scatter, in the $I-$band, of only $\pm 0.1\ mag$, systematic effects may exist. For example, a serious concern is whether there is any environmental

dependence of the relation. It has been suggested that a different metalicity of the host galaxy may significantly affect the zero-point of the relation and thus the determined distance. These effects can be taken into account and this method has proved to be fundamental in the recent determinations of $H_\circ$, because it provides the link between the primary galactic indicators and the *local* extragalactic ones, which then provide the calibration for other secondary indicators operating in much larger distances (cf. [61] and references therein).

In developing the distance scale, we now need effective indicators that can be used to very large distances. Other scaling relations have been found between a distance dependent (ex. brightness, diameter) and a distance independent (ex. rotational velocity, stellar velocity dispersion) quantity. It is evident that from such relations one can extract distance information. The main assumption in such a use of these scaling relations is that they are not environment-dependent (which has been shown to be a valid assumption). Such a relation for spiral galaxies is the *Tully-Fisher relation* [175], which relates the rotational velocity of a spiral to its total infrared luminosity: $L_{\rm ir} \propto V_{\rm rot}^4$ or its total blue luminosity: $L_{\rm b} \propto V_{\rm rot}^\alpha$ with $\alpha \sim 2.4 - 2.8$. It has a reasonable theoretical justification: Rotational velocities in spirals are related to mass according to

$$V_{\rm rot}^2 \propto \frac{M}{R} \tag{52}$$

Assuming that all spirals have the same surface brightness S, then

$$S \propto L/R^2 \Rightarrow L \propto R^2 \tag{53}$$

If the mass to light ratio is constant then

$$\frac{M}{L} \propto V_{\rm rot}^2 L^{1/2} \Rightarrow L \propto V_{\rm rot}^4 \tag{54}$$

For ellipticals a similar relation holds, the *Faber-Jackson* relation [60], which relates the absolute luminosity of the galaxy with the stellar velocity dispersion ($L \propto \sigma^{3-4}$) or a variant, the so-called $D_{\rm n} - \sigma$ *relation* (cf. [50]), which relates the diameter $D_{\rm n}$ of an elliptical (defined as that within which the mean surface brightness is 20.75 *mag arc sec*$^{-2}$ in B) to the stellar velocity dispersion σ: $D_{\rm n} \propto \sigma^x$ with $x \sim 1.2 - 1.3$. The typical accuracy of these distance estimations is $\sim 20\%$ and the usual assumption is that they do not evolve with redshift over the scales used, and that systematic effects can be corrected for. However, there are some indications for an evolution of the B-band *Tully-Fisher* relation in the interval studied $0.1 < z < 1$ [195].

Another very important distance indicator, which can be used to large distances, is the *Supernova SNIa brightness at maximum*. It is thought that the maximum luminosity of such supernovae (explosion of white dwarfs in binary systems which become gravitationally unstable - reaching the Chandrasekhar limit - due to the accretion of matter from the secondary - see [92]) is a Universal constant and since the intrinsic luminosity of a SNIa is high, they can be seen out to cosmological distances. Furthermore, a correlation was found between the

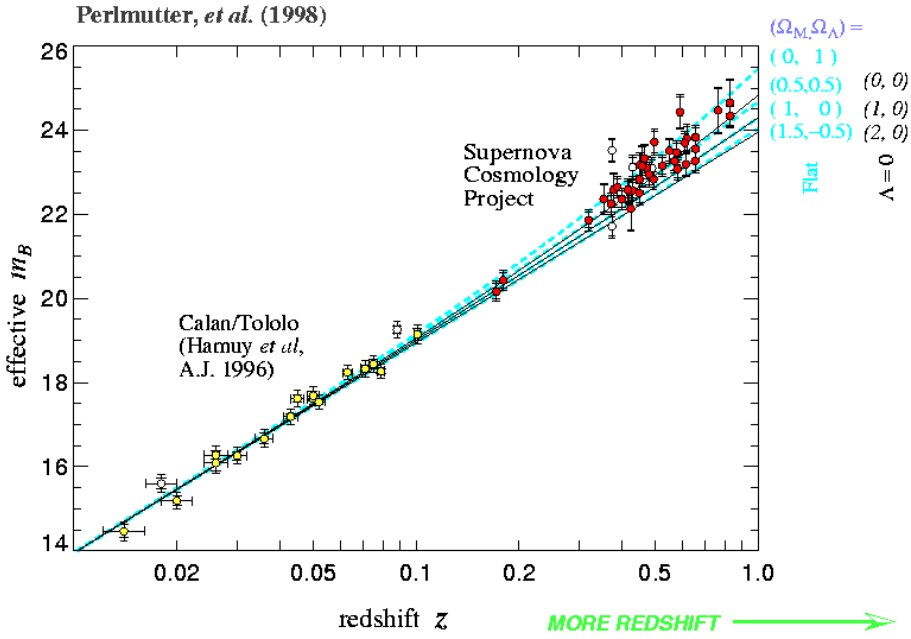

Fig. 5. The SN Ia Hubble diagram *vs* Cosmological model predictions (from [119] with permission).

supernova luminosity and the brightness decay time, which provides a further parameter that reduces the scatter in luminosity to ± 0.3 mags. Using this distance indicator one can construct the Hubble diagram to very large-distances and thus determine the deceleration of the Universe by mapping the region of the Hubble diagram that deviates from linearity. This has been recently achieved by two independent groups, the *Supernova Cosmology Project - SCP* [118] and the *High-z Supernova Search Team - HZT* [156], which have found that the derived Hubble diagram is that expected from a accelerating expansion, which can be provided by a non-zero cosmological constant (see Fig.5).

Although I do not plan to present all the secondary distance indicators, one that is potentially very important and susceptible to small uncertainties and systematics, is the *surface brightness fluctuation* method. This method is based on the fact that the discreteness of stars within galaxies depends on distance. This methods has an accuracy of $\sim 5\%$ in distance.

Direct Distance Indicators: Clusters of galaxies are filled with hot and transparent gas which can be fitted by a thermal Bremsstrahlung spectrum with $T \sim 5 \times 10^7 - 10^8\ K$ (covering a range of $2 \sim 8$ KeV). The physics of the hot intercluster gas provides the means of measuring directly the distance of clusters, without need of intermediate steps. This method is based on the so called *Sunyaev-Zeldovich effect* which is the distortion of the original CMB spectrum,

by the Compton scattering to higher energies of the CMB photons from the hot electrons of the plasma (for recent reviews see [131], [17]). This distortion decreases the brightness of the CMB spectrum at the longer wavelength range while it increases the photon energies in the shorter wavelength range. Lets assume a cluster of radius R at a distance D, subtending an angular separation θ on the sky. The change of the CMB brightness temperature is proportional to the line integral of electron number density through the cluster:

$$\frac{\Delta T}{T} \propto -\int T_{\rm e}(l)\, n_e \,{\rm d} \tag{55}$$

then from isothermality we get $\Delta T/T \propto T_{\rm e}\, n_{\rm e}\, R$. Furthermore the luminosity of the Bremsstrahlung radiation together with the assumption of isothermality, gives:

$$L_{\rm x} \propto \int n_{\rm e}^2\, T_{\rm e}^{1/2}(r)\, 4\pi r^2\, {\rm d}r = n_{\rm e}^2\, T_{\rm e}^{1/2}\, R^3 \tag{56}$$

From (56), the observed X-ray flux ($F_{\rm x} \propto L_{\rm x}/D^2$) and $R = \theta D$ we have:

$$F_{\rm x} \propto n_{\rm e}^2\, T_{\rm e}^{1/2}\, \theta^3\, D \propto \left(\frac{\Delta T}{T}\right)^2 \frac{\theta}{T_{\rm e}^{3/2}\, D} \tag{57}$$

and solving for D we get:

$$D \propto \left(\frac{\Delta T}{T}\right)^2 \frac{\theta}{T_{\rm e}^{3/2} F_{\rm x}}$$

Therefore measuring $F_{\rm x}$, θ, $T_{\rm e}$ we obtain an absolute determination of the cluster distance. The temperature, $T_{\rm e}$, can be measured either from the shape of the X-ray continuum or from line emission (especially of iron). Note however, that we have assumed sphericity, isothermality and a smooth distribution of $n_{\rm e}$. Most clusters are flattened (cf. [12]), and show significant substructure apparent in the optical and X-ray images. In such clusters the above procedure may provide highly uncertain and biased distance estimates (cf. [77]). A recent study of ~ 100 clusters has shown that once cooling flows are taken into account, isothermal profiles fit well $\sim 90\%$ of the clusters ([185], but see also [45]).

2.4 The Value of $H_\circ$ and the Age of the Universe

The immense effort that has been put towards the goal of determining $H_\circ$, with an accuracy of a few %, has recently come to fruition with different methods providing consistent (within $< 10\%$) values. In Table 1, I present a list of some of the most recent determinations of $H_\circ$. Note that there are 3 different measurements based on SNIa, giving different values of $H_\circ$. Although many of the SNIa they use are common, the difference is most probably attributable to the different local calibrations that they employ. Thus, the differences in their derived $H_\circ$'s should reflect the *systematic* uncertainty introduced by the different

local calibrations and it is indeed comparable to the systematic uncertainty that the individual studies have estimated.

The method in the last row of Table 1 is based on *gravitational lensing* (cf. [20]). The basic principle behind this method is that there is a difference in the light travel time along two distinct rays from a source, which has been gravitationally lensed by some intervening mass. The relative time delay (Δt), between two images of the source, can be measured if the source is variable. Then it can be shown that the Hubble constant is just:

$$H_\circ = \mathcal{C}\frac{\Delta\theta^2}{\Delta t} \tag{58}$$

where $\Delta\theta$ is the image separation and $\mathcal{C}$ is a constant that depends on the lens model. Although, this method has well understood physical principles, still the details of the lensing model provide quite large uncertainties in the derived $H_\circ$.

A crude N-weighted average of the different $H_\circ$-determinations in Table 1 gives:

$$H_\circ = 68 \pm 6 \quad \text{km sec}^{-1}\ \text{Mpc}^{-1}$$

where the uncertainty reflects that of the weighted mean (the individual uncertainties have not been taken into account). However, there seems to be some clustering around two preferred values ($H_\circ \simeq 60$ and $\simeq 72$ km s^{-1} Mpc^{-1}) and thus the above averaging provides biased results. More appropriate is to quote the median value and the 95% confidence limits:

$$H_\circ = 72^{+4}_{-13} \quad \text{km sec}^{-1}\ \text{Mpc}^{-1}\ , \tag{59}$$

The anisotropic errors reflect the non-Gaussian nature of the distribution of the derived $H_\circ$-values. Note that the largest part of the individual uncertainties, presented in Table 1, of all methods except the last two, are *systematic* because they rely on local calibrators (like the distance to the LMC), which then implies that a systematic offset of the local zero-point will "perpetuate" to the secondary indicators although internally they may be self-consistent. A further source of systematic errors is the peculiar velocity model, used to correct the derived distances, which can easily introduce $\sim 7\%$ shifts in the derived $H_\circ$ values [146] [190].

With the value (59), we obtain a *Hubble* time, $t_{\rm H}$, equal to:

$$t_{\rm H} = H_\circ^{-1} = 1.36^{+0.30}_{-0.06} \quad \text{Gyr's} \tag{60}$$

the uncertainties reflecting the 95% confidence interval.

It is trivial to state that the present age of the Universe $t_\circ$, should always be larger than the age of any extragalactic object. A well known problem that has troubled cosmologists, is the fact that the predicted age of the Universe, in the classical Einstein de-Sitter Cosmological Model is smaller than the measured age of the oldest globular clusters of the Galaxy. This can be clearly seen from (60) and

$$t_\circ^{\rm EdS} = \frac{2}{3}t_{\rm H} \simeq 0.9^{+0.20}_{-0.07} \quad \text{Gyr's} \tag{61}$$

Table 1. Some recent determinations of the Hubble constant, based on different methods.

Method	N	$H_\circ$	$\langle z \rangle$	reference
Cepheid	23	75±10	0.006	Freedman et al 2001
2-ary methods	77	72±8.0	$\lesssim 0.1$	Freedman et al 2001
IR SBF	16	76±6.2	0.020	Jensen et al. 2000
SN Ia	36	73±7.3	$\lesssim 0.1$	Gibson & Brook 2001
SN Ia	35	59 ± 6	$\lesssim 0.1$	Parodi et al 2000
SN Ia	46	64 ± 7	$\lesssim 0.1$	Jua et al 1999
CO-line T-F	36	60±10	< 0.11	Tutui et al 2001
S-Z	7	66±15	< 0.1	Mason et al 2001
Grav. Lens	5	68 ± 13		Koopmans & Fassnacht 2000

and although the latest estimates of the globular cluster ages have been drastically decreased to [84]:

$$t_{\rm gc} \simeq 12.5 \quad \text{with 95\% lower/upper limit is 11/16 Gyr's .}$$

One should then add the age of the formation of the globular clusters and assuming a redshift of formation $z \simeq 5$ then this age is $\sim 0.6 - 0.8$ Gyr's which brings the lower 95% limit of $t_{\rm gc}$ to ~ 11.6 Gyr's (see however [30] for possible formation at $z \gtrsim 10$). It is evident that there is a discrepancy between $t_\circ$ and $t_{\rm gc}$. This discrepancy could however be bridged if one is willing to push in the right direction the 95% limit of both $t_{\rm H}$ and $t_{\rm gc}$.

However, other lines of research point towards the age-problem. For example, if at some large redshift we observe galaxies with old stellar populations, for which we know the necessary time for evolution to their locally "present"state, then we can deduce again the age of the Universe. In an EdS we have $R \propto t^{2/3}$ and thus we have:

$$t_\circ = t_{\rm z}(1+z)^{3/2} \tag{62}$$

Galaxies have been found at $z \simeq 3$ with spectra that correspond to a stellar component as old as ~ 1.5 Gyr's, in their local rest-frame. From (62) we then have that $t_\circ \simeq 12$ Gyr's, in disagreement with the EdS age (61).

This controversy could be solved in a number of ways, some of which are:

- invoking an open ($\Omega < 1$) cosmological model,
- assuming that we live in a local underdensity of an EdS Universe,
- invoking a flat model with $\Omega_\Lambda > 0$.

The first possibility is in contradiction with many observational data and most importantly with the recent CMB experiments (BOOMERANG, MAXIMA and DASI), which show that $\Omega = 1$ (see [44] [43] [90] [164] [130]).

The second possibility [173] can solve the age-problem by assuming that we live in a local underdense region that extends to quite a large distance, which would then imply that the measured local Hubble constant is an overestimate

of the global one by a factor:

$$\frac{\delta H}{H} = \frac{\Omega_{\rm m}^{0.6}}{3b}\frac{\delta N}{N}$$

where the bias factor b, is the ratio of the fluctuations in galaxies and mass. To reduce the Hubble constant to a comfortable value to solve the age problem, say from 72 to 50 km sec^{-1} Mpc^{-1}, one then needs $\delta N/N \simeq -0.9/b$. Values of b are highly uncertain and model dependent, but most recent studies point to $b \sim 1$ (cf. [88]) which would then mean that we need to live in a local very underdense region, something that is not supported by the linearity of the Hubble relation out to $z \lesssim 0.03$ (cf. [64]) or out to $z \lesssim 0.1$ (cf. [171]). This is not to say that we are not possibly located in an underdense region, but rather that this cannot be the sole cause of the *age*-problem [193].

Thus we are left with the last possibility of a Universe dominated by vacuum energy (a Universe with $\Omega_\Lambda > 0$ - see section 1.3). If we live in the accelerated phase (see Fig.1) we will measure:

$$H(t_\circ) > H(t) \qquad \text{with } t_\circ > t$$

ie., a larger Hubble constant, and thus smaller Hubble time as we progress in time, resolving the age-problem. In fact we have strong indications (see next section), from the SNIa results, which trace the Hubble relation at very large distances (see section 3.2), and from the combined analysis of CMB anisotropy and galaxy clustering measurements in the 2dF galaxy redshift survey [54], for a flat Universe with $\Omega_\Lambda \simeq 0.7$. Then from (23) we obtain the age of the Universe in such a model:

$$t_\circ^\Lambda = 1.446 \times t_\circ^{\rm EdS} = 1.31^{+0.28}_{-0.11}\ {\rm Gyr's}$$

Indeed the resolution of the *age*-problem gives further support to the $\Omega_\Lambda > 0$ paradigm.

3 Determination of the Matter/Energy Density of the Universe

The existence of large amounts of Dark Matter in the universe, manifesting itself through its gravitational effects, is a well established fact, although the precise amount has been a matter of a lively debate through the years. Attempts to identify the DM as normal *baryonic* matter has failed, mostly due to the nucleosynthesis constraints imposed by the successful hot Big-Bang model and the large temperature fluctuations of the CMB that it predicts in a flat Universe ($\frac{\delta T}{T} \sim \frac{1}{3}\frac{\delta \rho}{\rho}$). Possibly some of the DM could be neutral hydrogen, in the form of Lyman-α clouds, but it is estimated that it could contribute only $\Omega \lesssim 0.01$. Similarly, the possible solid form of baryonic material (eg. dust grains, *Jupiters*, dwarfs with $M \lesssim 0.08 M_{\odot}$ or neutron stars) would contribute little to Ω.

Two recent determinations of the deuterium abundance, which combined with the BBN (Big-Bang Nucleosynthesis) predictions, give the total baryonic mass in the universe, have provided slightly discrepant results (see reviews [107], [163]), covering the range:

$$0.005 \lesssim \Omega_{\rm B} h^2 \lesssim 0.024 \tag{63}$$

and therefore for $h = 0.72$ we have: $0.01 \lesssim \Omega_{\rm B} \lesssim 0.046$. However, the recent analysis of the results from the BOOMERANG CMB experiment have provided a value mostly compatible with the lower deuterium abundance and thus higher $\Omega_{\rm B} h^2$ value (see further below).

In this section we present a variety of methods used to estimate either the total mass/energy density of the Universe or its mass density, $\Omega_{\rm m}$.

3.1 The CMB fluctuation spectrum

The most straight forward approach to estimate the total matter and energy density of the Universe (ie., the total Ω) is by means of the measurement of the fluctuation spectrum of the CMB. Before recombination at $z \lesssim 1100$, the baryons and photons are tightly coupled, oscillating acoustically due to gravity (on sub-horizon scales). Only after recombination do the acoustic oscillations stop and the density fluctuations grow. The fluctuations emerging from the last scattering surface are a series of peaks and troughs [169] and as the different wave-lengths are projected to different angular scales on the last scattering surface and depending on the underlying cosmological model, they produce a characteristic structure of peaks on the CMB power spectrum (for a recent review see [98] and references therein). This method is in effect based in measuring the angular extent of a physical scale on the last scattering surface. The curvature of space enters through the angular distance to the last scattering surface. Therefore, the same physical scale will be projected to a smaller angular scale on the CMB sky in a positively curved background, while it will be projected to a larger angular scale in a flat or to an even larger scale in a negatively curved background space.

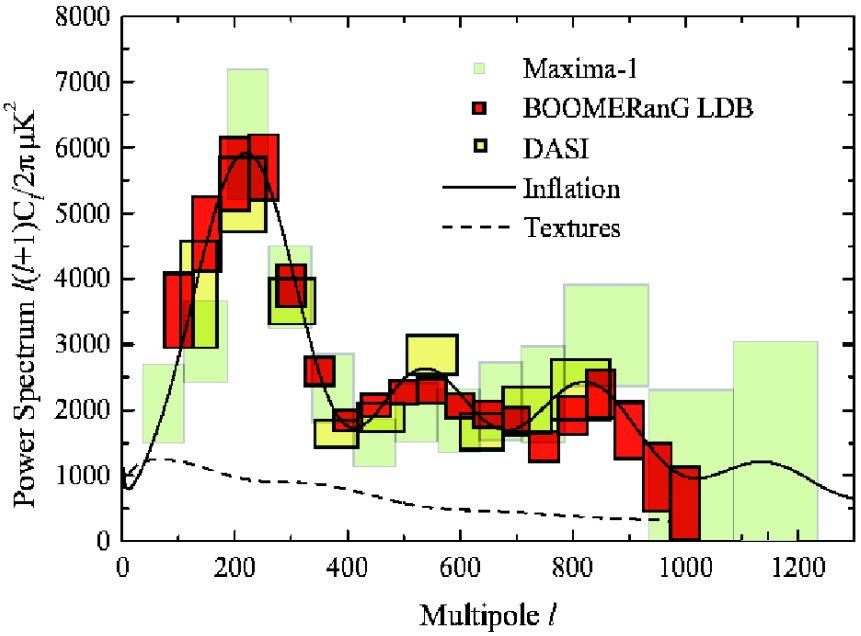

Fig. 6. CMB spectrum from the BOMMERANG, MAXIMA and DASI experiments with the error boxes of the measurements. The predictions of the popular inflationary model and one non-Gaussian (global texture) model (from [98] with permission).

To define the CMB power spectrum one starts by expanding the temperature fluctuations of the CMB sky in spherical harmonics:

$$\frac{\delta T}{T}(\theta,\phi) = \sum_{\ell=1}^{\infty} \sum_{m=-\ell}^{m=\ell} a_{\ell m} Y_{\ell m}(\theta,\phi) \ , \tag{64}$$

then if the fluctuations are Gaussian, the 2-point correlation function contains all the statistical information, and can be defined as:

$$\left\langle \left(\frac{\delta T}{T}\right)^2 \right\rangle = \frac{1}{4\pi} \sum_{\ell} (2\ell+1)\, C_\ell\, W_\ell\, P_\ell(\theta,\phi) \ . \tag{65}$$

where W_ℓ is the window function representing the beam characteristics of the experimental apparatus used to observe the CMB sky, while the average is over all positions on the sky. One then invokes the ergotic theorem, ie, that the above average is equivalent to being over different realizations of our Universe. Then assuming random phases one can define the CMB power spectrum C_ℓ as the ensemble average of the coefficients $a_{\ell m}$:

$$C_\ell = \langle |a_{\ell m}|^2 \rangle$$

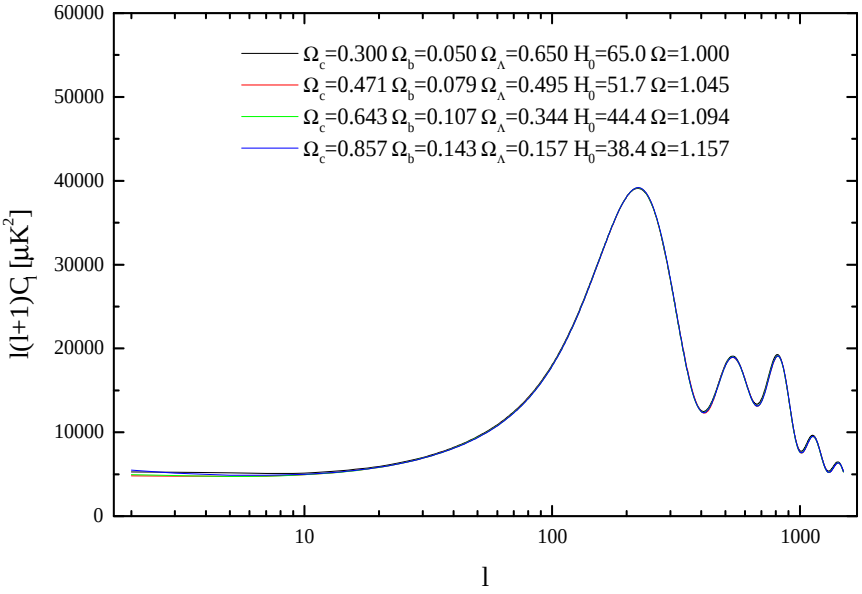

Fig. 7. Different combinations of the cosmological parameters can result in the same CMB power-spectrum - degeneracy problem (form [99] with permission)
.

The different cosmological parameters will reflect onto a different structure of peaks in the structure of the CMB power spectrum. The position of the first peak is determined by the global mass/energy density of the Universe and the dependence of $\ell_{\rm peak}$ on Ω can be approximated by:

$$\ell_{\rm peak} \sim \frac{220}{\sqrt{\Omega}} \tag{66}$$

Note however, that this approximation is not correct in Λ–dominated universes and small corrections should be applied (cf. [99]). Many recent experiments like the BOMMERANG, MAXIMA and DASI (cf. [44], [43], [90] [164] [130]) find:

$$\Omega_{\rm tot} \simeq 1.02\ (\pm 0.07)$$

Many other cosmological parameters (for example $\Omega_{\rm m}$, Ω_Λ, $H_\circ$, baryon content of the universe, the spectral index n of the inflationary perturbation spectrum, etc) affect the structure of the peaks, beyond the first one (cf. [71]). Determining the CMB spectrum up to a few thousand ℓ's can put strong constraints on these parameters. Current experiments trace the CMB spectrum up to $\ell \sim 1000$ and indeed they have detected two more significant peaks at roughly $\ell \sim 540$ and 840 [43] (see Fig.6).

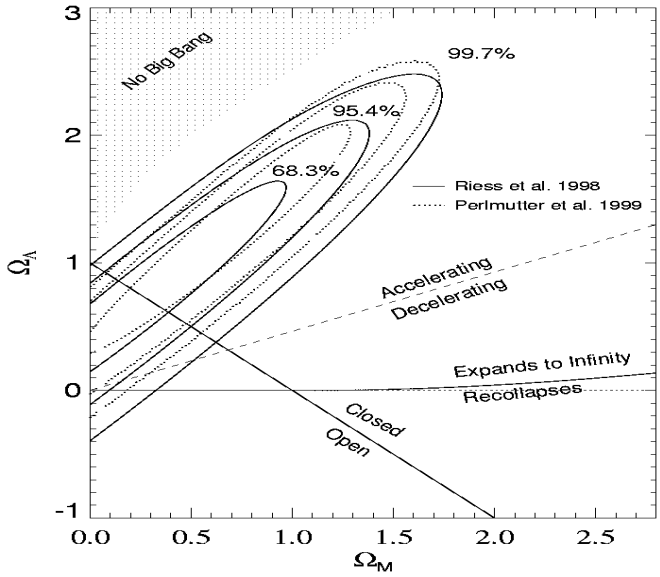

Fig. 8. Confidence intervals for $(\Omega_{\rm m} - \Omega_\Lambda)$ from the SCP and HZT results (from [136] with permission).

Note however, that different combinations of the cosmological parameters can conspire to produce exactly the same CMB spectrum; this is the so called degeneracy problem (see Fig.7) and therefore in order to provide limits to these cosmological parameters one needs to assume priors and/or constrain different combinations of these parameters. However, the more accurate the derived CMB spectrum the weaker the necessary priors[2].

The latest data and CMB spectrum analysis provides very stringent constraints to the baryon content of the Universe: $\Omega_{\rm B}h^2 \simeq 0.022^{+0.004}_{-0.003}$, consistent with the primordial nucleosynthesis constraints (see 63), and to the spectral index of the power spectrum of primordial perturbations: $n \simeq 0.96 \pm 0.1$ [43]. Furthermore, combined analyses with other cosmological data, can be used to break the above mentioned degenerecies (see below).

3.2 The Hubble diagram with SNIa

As we have already discussed in section 2.3, the Hubble diagram of supernovae SNIa can be used not only to determine the Hubble constant (at relatively low redshifts) but also to trace the curvature of the Hubble relation at high redshifts (see [136] and references therein).

[2] With the new CMB experiments - MAP and PLANCK - the CMB power spectrum will be determined to an unprecedent detail, providing extremely accurate values for more than 10 cosmological parameters [160].

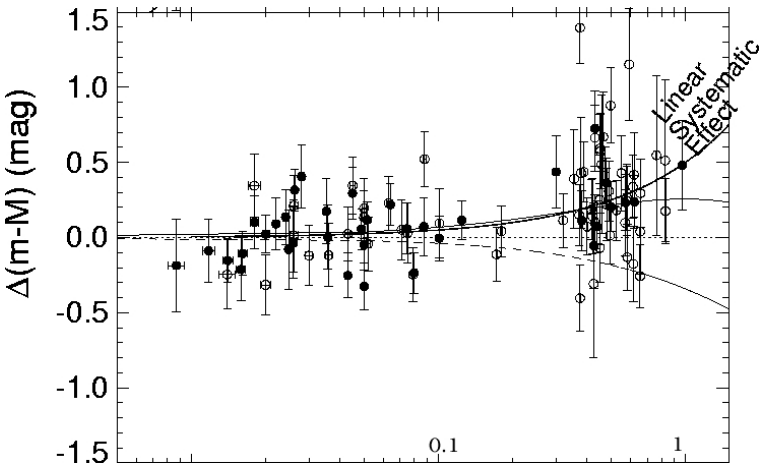

Fig. 9. Distance modulus residuals after subtracting an open $\Omega_m = 0.3$ Hubble relation (straight dashed line). The flat $\Omega_\Lambda = 0.7$ model is the thin curved line while the systematic effect is the thick label line (from [136] with permission).

The two groups working laboriously on this subject (SCP and HZT) have found consistent results, by which the distant SNIa's are dimmer on average by 0.2 mag than what expected in a flat EdS model, which translates in them being $\sim 10\%$ further away than expected ([119], [135]). This implies that we live in an accelerating phase of the expansion of the Universe, a fact that supports a non-zero cosmological constant. The confidence intervals that their results put in the $\Omega_m - \Omega_\Lambda$ plane are shown in Fig.8. These results can be quantified by the following expression [119]:

$$0.8\Omega_{\rm m} - 0.6\Omega_\Lambda = 0.2\ (\pm 0.1)$$

Together with the CMB fluctuation spectrum results we obtain:

$$\Omega_{\rm m} \simeq 0.29 \quad \Omega_\Lambda \simeq 0.71\ .$$

However, since our understanding of the physics of SNIa'a is not complete (cf. [92], [91]) there could be some systematic effect, correlated with distance (eg. evolution), which could explain the dimming of the distant SNIa's and thus alleviate the $\Omega_\Lambda > 0$ interpretation. In Fig.9 we show the distance modulus residuals after subtracting an open $\Omega_{\rm m} = 0.3$ Hubble relation. The systematic distant-dependent effect mimics the accelerated expansion Hubble relation out to $z \sim 0.8 - 1$. Beyond $z \sim 1$ the two relations depart due to the fact that the accelerated phase has to first pass from a decelerating one (see discussion in section 1.3) and this could provide a strong test for the possible distant dependent systematics. In fact, the recent discovery of the furthest known supernova (SN 1997ff) at a redshift of $z \sim 1.7$ [137], has provided evidence of the decelerating phase of the presently accelerating Universe (however, more very high-z supernovae are necessary to confirm this extraordinary result).

3.3 Clustering of Galaxies, Clusters & QSO's

If we assume a continuous density field of extragalactic objects, $\rho(\boldsymbol{r})$, with mean $\overline{\rho}$, we define the fluctuations of the field at position $\boldsymbol{x}$ as:

$$\delta(\boldsymbol{x}) = \frac{\rho(\boldsymbol{x}) - \overline{\rho}}{\overline{\rho}} \ , \tag{67}$$

Obviously we have that $\langle \delta(\boldsymbol{x}) \rangle = 0$. The correlation function is defined as:

$$\xi(r) = \langle \delta(\boldsymbol{x}) \delta(\boldsymbol{x}+\boldsymbol{r}) \rangle = \frac{\langle \rho(\boldsymbol{x}+\boldsymbol{r}) \rho(\boldsymbol{x}) \rangle - \overline{\rho}^2}{\overline{\rho}^2} \ . \tag{68}$$

and quantifies the extend to which the density fluctuations at a given point are correlated to those at a distance r. The value of 2-point correlation function at zero-lag is therefore the variance of the random process:

$$\xi(0) = \langle \delta^2(\boldsymbol{x}) \rangle$$

which measures the excursions of the density about its mean value. However, this is not a well defined quantity because usually the fluctuation field is smoothed to some resolution, say R. We then evaluate the variance of this field as $r \longrightarrow 0$ (see 71 below).

In many problems it is convenient to work in wave-number space. The Fourier transform of $\delta(\boldsymbol{x})$ is:

$$\delta_{\boldsymbol{k}} = \int \delta(\boldsymbol{x}) e^{i\boldsymbol{k}\cdot\boldsymbol{x}} \mathrm{d}^3\boldsymbol{x} \tag{69}$$

and it is convenient to separate $\delta_{\boldsymbol{k}}$ in modulus and argument:

$$\delta_{\boldsymbol{k}} = |\delta_{\boldsymbol{k}}| e^{i\epsilon_{\boldsymbol{k}}} \ ,$$

where $\epsilon_{\boldsymbol{k}}$ are the phases (usually assumed to be randomly distributed in $[0, \pi)$, although the non-linear evolution of structure introduces phase correlations, cf. [33]). The variance of the amplitudes is the power spectrum:

$$P(\boldsymbol{k}) \equiv \langle |\delta_{\boldsymbol{k}}|^2 \rangle$$

which is the Fourier transform of the correlation function (*Wiener-Khinchin* theorem):

$$P(\boldsymbol{k}) = \int \xi(\boldsymbol{r}) e^{i\boldsymbol{k}\cdot\boldsymbol{r}} \ \mathrm{d}^3\boldsymbol{r} \tag{70}$$

and with inverse transform: $\xi(\boldsymbol{r}) = (2\pi)^{-3} \int P(\boldsymbol{k}) e^{-i\boldsymbol{k}\cdot\boldsymbol{r}} \mathrm{d}^3\boldsymbol{k}$. At the origin $\boldsymbol{r} = 0$ we obtain

$$\xi_{\mathrm{R}}(0) = \langle \delta^2_{\mathrm{R}}(\boldsymbol{x}) \rangle = \frac{1}{(2\pi)^3} \int_{\boldsymbol{k}} P(\boldsymbol{k}) \ W^2(kR) \mathrm{d}^3\boldsymbol{k} \tag{71}$$

where W is the window function function that reflects the filtering of the field. The power spectrum is the contribution of modes of wavenumber $\boldsymbol{k}$ to the total variance, per unit volume of wavenumber space. If the fluctuation field is a

Gaussian Random Field, then the power-spectrum contains all the statistical information of the fluctuations. A similar formulation is applicable also in the two dimensional case (where the density field is on the surface of a sphere - the sky). Only that instead of the Fourier transform we use the Spherical Harmonic transform.

Although I will not enter in the details of how to estimate the power spectrum of some distribution of extragalactic objects, I will only note that a good estimation of the window function (containing the survey boundaries, obscuration, radial selection function and instrumental biases for example) is necessary in order to get a reliable power-spectrum determination.

A further ingredient that complicates considerably matters is the so called biasing of the galaxies, or in general of any mass-tracer population, with respect to mass [79]. The usual relation, assumed between the mass-tracer fluctuations ($\delta_{\rm tr}$) and the underline mass fluctuation field, is encapsulated in the bias factor b:

$$\delta_{\rm tr} = b\ \delta_{\rm m} \tag{72}$$

and therefore we have that the galaxy (tracer) power spectrum is

$$P_{\rm tr}(k) = b^2 P_{\rm m}(k)$$

It has been shown that the linear biasing model (72) is a good approximation, at least on scales were non-linear gravitational effects are weak (see [106] and references therein).

Within the inflationary paradigm the initial fluctuations, in the early universe, that gave rise to the observed large-scale structure today, are *adiabatic* and *Gaussian* and therefore one can characterize these fluctuations completely using the above tools. The power spectrum of such initial fluctuations is:

$$P_{\rm in}(k) = Ak^n$$

usually with $n = 1$ (*Harrison-Zeldovich* spectrum), and A its amplitude. The different fluctuation damping mechanisms, operating during the radiation dominated area, modify $P_{\rm in}(k)$. These effects can be encapsulated in the *transfer function*, $T(k)$ and today's linear fluctuation spectrum has the form [8]:

$$P(k) = T^2(k) P_{\rm in}(k)$$

In the linear regime (while fluctuations $\ll 1$) the power spectrum shape is preserved, because each Fourier mode evolves independently.

I will now concentrate on a few methods, based on the clustering of galaxies and QSO's, and I will present only very recent results. The subject is extremely rich, many have laboriously worked towards attaining the goal of pining down the different cosmological parameters and I hope that they will forgive me for not being able to mention the vast literature on the subject.

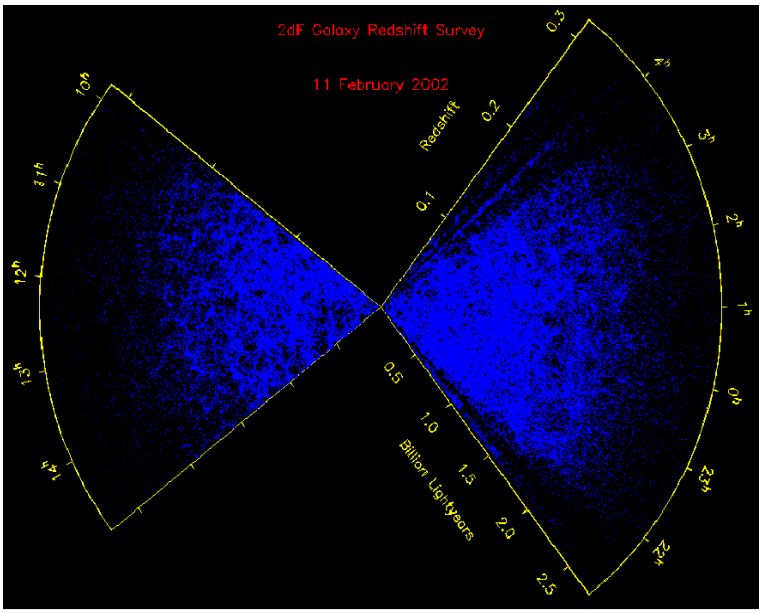

Fig. 10. Pie-diagram of the latest 2dF release, containing 160000 galaxies (with permission from the 2DFGRS TEAM).

The Shape of $P(k)$: The popular Cold Dark Matter (CDM) model has a $T(k)$ parametrised by the so-called *shape-parameter*, Γ, which characterizes the shape of the $P(k)$ and has the form [168]:

$$\Gamma = \Omega_{\rm m} h \, \exp\left[-\Omega_{\rm B}(1+\sqrt{2\,h}/\Omega_{\rm m})\right] \tag{73}$$

We see that measuring the the power-spectrum of extragalactic populations and estimating Γ we can put constraints on the combination of the cosmological parameters: $\Omega_{\rm m}$ and h ($\Omega_{\rm B}$ affects weakly Γ).

The recent 2dF survey [37] has measured already measured more than 160000 galaxy and 10000 QSO redshifts, which constitute it the largest spectroscopic catalogue of extragalactic objects. A number of recent papers have estimated the galaxy and QSO power-spectra providing important constraints on the Γ parameter. From the $P(k)$ of galaxies [117] it was found that there is a degeneracy between the $\Omega_{\rm m}h$ and $\Omega_{\rm B}/\Omega_{\rm m}$, which if broken (using the CMB or BBN results) provide the following constraints:

$$\Omega_{\rm m}\, h \simeq 0.2(\pm 0.03) \quad \Omega_{\rm B} \simeq 0.15(\pm 0.07)\Omega_{\rm m}$$

which for $h = 0.72$ means that $\Omega_{\rm m} = 0.28$. The analysis of the QSO $P(k)$ [70] showed a somewhat smaller value but still consistent within the statistical uncertainties:

$$\Gamma \simeq 0.1(\pm 0.1)$$

Similar results come from the SSDS photometric survey [165] which contains $1.5{\times}10^6$ galaxies with redshifts up to ~ 0.4. The angular power-spectrum analysis, after inverting to 3D using Limber's integral equation, give [47] [170]:

$$\Gamma \simeq 0.14^{+0.11}_{-0.06} \;\; 95\% \text{ C.L.}$$

Obviously, all these results support a low $\Omega_{\rm m}$ universe.

Redshift Space Distortions: As we have already discussed in section 2, the measured expansion velocity of an extragalactic object contains also the contribution of the local gravitational field. The peculiar velocities will distort the apparent 3D distribution of the extragalactic objects, a fact which will manifest itself in the 2-point correlation function, when plotted as a function of the transverse and radial pair separation. The redshift space correlation function is related to the real space, under a few assumptions; see [78], according to:

$$\xi_{\rm s}(r) = \xi_{\rm r}(r)\left(1+\frac{2}{3}\beta+\frac{1}{5}\beta^2\right) \tag{74}$$

where $\beta = \Omega_{\rm m}^{0.6}/b$. By estimating the angular power-spectrum, C_ℓ, or its Fourier transform $w(\theta)$, and then inverting it to 3D via Limber's equation, one has an unaffected, by redshift space distortions, measure of these parameters. Then using (74) and the measured $\xi_{\rm s}(r)$ one can place constraints on β. Such an analysis of the 2dF galaxy survey gave [113]:

$$\Omega_{\rm m} \simeq 0.25(\pm 0.06)\, b_{\rm op}^{-1.66}$$

A subsequent analysis, using a different method, provided very similar results [172]:

$$\Omega_{\rm m} \simeq 0.3(\pm 0.15)\, b_{\rm op}^{-1.66}$$

The corresponding QSO survey [108] did not provide very stringent constraints (ie., the EdS model was rejected only at a 1.4σ level), however their best fit gives:

$$\Omega_{\rm m} \simeq 0.21(\pm 0.15)\, b_{\rm QSO}^{-1.66}$$

Joint Likelihoods: Alot of recent interest was generated by the understanding that joining the analyses of different data sets, one may break the degeneracies between the different cosmological parameters (cf. [182] [53] [29] [181]). Especially joining the CMB, SNIa and large-scale clustering results may lead to strong constraints on more than 8 cosmological parameters (see however [87] for many subtleties involved).

The joint analysis [54] of the 2dF galaxy $P(k)$ and the CMB data have provided another strong indication for a positive cosmological constant, independent of the SNIa results, with a 2σ range:

$$0.65 < \Omega_\Lambda < 0.85$$

Furthermore, some of the other constraints are: $0.17 < \Omega_{\rm m} < 0.31 \quad \text{for } h = 0.72$, $0.6 < h < 0.86$.

3.4 M/L observations

Each astronomical object is characterized by a quantity called Mass-to-Light ratio, M/L. A convenient scaling of M/L is done by using the value of the solar neighbourhood, $M_\odot/L_\odot$. Then, observing $M/L > M_\odot/L_\odot$ would imply the existence of DM of unknown composition and origin. Note that in most cases the evidence for $M/L > M_\odot/L_\odot$ comes from the gravitational effects of the DM. Different classes of extragalactic objects (galaxies, clusters, etc) are characterized by different M/L, indicating that possibly a different fraction of the total mass of each type of object is *Dark*.

Estimating the universal luminosity density (see further below) and using the derived M/L values of each class of extragalactic object we can estimate its contribution to the total $\Omega_{\rm m}$. Furthermore, if the estimated M/L is representative of the global universal value, then we can derive the overall value of $\Omega_{\rm m}$.

I will present below the basic ideas behind the determination of M/L for the different extragalactic populations.

Spiral Galaxies: The Rotation curves of spirals (see Fig.10) are obtained by measuring Doppler-shifts of emission lines in HII regions, at radio wavelengths using the 21-cm emission line of neutral Hydrogen or using the CO-line and in the latter cases the rotation curve is measured at several times the optical radius of a galaxy (for a recent review see [162]).

One would expect the rotation curve to fall roughly as the surface brightness and beyond a few length-scales to fall as $v_{\rm rot} \propto r^{-1/2}$ (because most of the mass is rather centrally located) which is not observed. The rotation curves are found to be flat as far as they can be observed. From simple Newtonian Physics we have that:

$$v_{\rm rot} \approx \left(\frac{GM}{r}\right)^{1/2}$$

and since $v_{\rm rot} \propto$ constant, we have that $M(r) \propto r$, ie., mass increases linearly with distance beyond its optical radius, an indication for the presence of *dark matter*. The average value of M/L found for spiral galaxies out to ~ 20 kpc, is:

$$M/L \sim 10 \pm 2 M_\odot/L_\odot \tag{75}$$

Note that the M/L value is an increasing function of outer radius, implying the existence of an extended dark matter halo (cf. [3]).

Elliptical Galaxies: In principle one can invoke a similar method with that of the spirals, if instead of the rotational velocity, the stellar velocity dispersion is used. The amplitude of this velocity measure is dictated by the gravitational potential of the elliptical and thus the virial theorem can be used to determine its total gravitating mass. However, stellar orbits are highly uncertain and the velocity dispersion ellipsoid may not be isotropic (see discussion in [16]).

Luckily, elliptical galaxies contain very hot gas ($T \sim 5 \times 10^6$ K) which emits X-rays. This gas constitutes about 10% of the observed mass in stars. For a

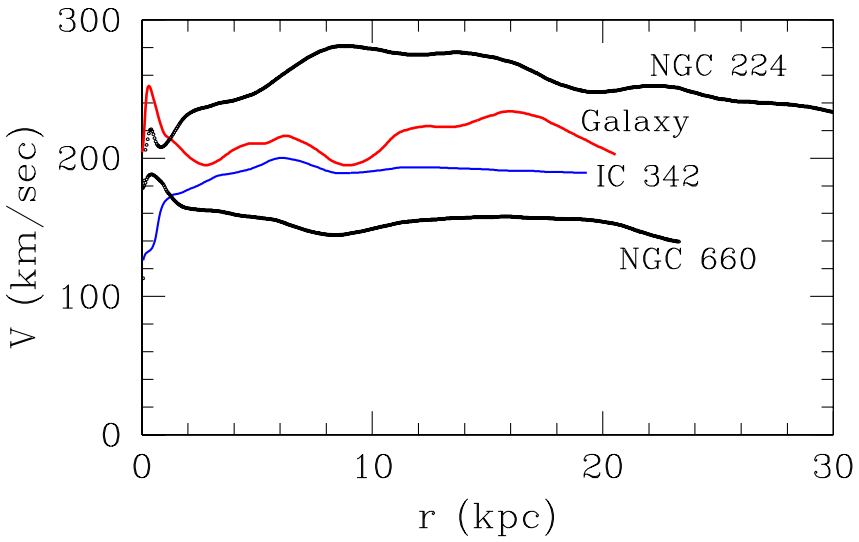

Fig. 11. Rotation curves of 4 spiral galaxies, one of which is the Galaxy (data taken from [161]).

spherically symmetric galaxy in hydrostatic equilibrium ($\boldsymbol{v} = 0$) we have from *Euler's* equation that:

$$\frac{\partial \boldsymbol{v}}{\partial t} + (\boldsymbol{v} \cdot \nabla)\, \boldsymbol{v} = -\frac{1}{\rho}\nabla p - \nabla \Phi \Longrightarrow$$

$$\frac{\mathrm{d}p}{\mathrm{d}r} = -\frac{GM(\leq r)\rho}{r^2}\ ,$$

Using the ideal gas law ($p = \rho k_{\mathrm{B}} T/m$) with m the molecular mass and k_{B} the Boltzmann constant, we obtain that:

$$M(\leq r) = \frac{k_{\mathrm{B}} T r}{\mu m_{\mathrm{p}} G}\left(-\frac{\mathrm{d}\ln\rho}{\mathrm{d}\ln r} - \frac{\mathrm{d}\ln T}{\mathrm{d}\ln r}\right) \tag{76}$$

where T is the gas temperature, m_{p} is the proton mass and μ is the mean molecular weight. Therefore if we measure the temperature and density profiles we can find the total mass distribution $M(< r)$. Finally the average mass-to-light ratio from this class of objects, out to ~ 20 kpc, is:

$$M/L \sim 25 \pm 5 M_{\odot}/L_{\odot}\ . \tag{77}$$

Groups of Galaxies: Groups of galaxies containing a few galaxies (3 - 10) are usually considered bound (due to the high density of galaxies). Then, according to the Virial theorem ($2T + U = 0$), a group with N galaxies having velocity

and position vectors (relative to the centre of mass of the group) $\boldsymbol{v}_{\rm i}$ and $\boldsymbol{r}_{\rm i}$ respectively, has:

$$\sum_{\rm i=1}^{\rm N} m_{\rm i} v_{\rm i}^2 = \sum_{\rm i=1}^{\rm N} \sum_{\rm j<i} \frac{G m_{\rm i} m_{\rm j}}{|\boldsymbol{r}_{\rm i} - \boldsymbol{r}_{\rm j}|} \ .$$

However what we measure is not $v_{\rm i}$ but only the line-of-sight component of the the velocity $u_{\rm i}$. Assuming isotropic orbits then $v_{\rm i}^2 \simeq 3\langle u_{\rm i}^2 \rangle$. Assuming that the mass-to-light ratio of each member galaxy is the same, $m_{\rm i}/L_{\rm i} = M/L$, we obtain:

$$\frac{M}{L} = \frac{3\pi}{2G} \frac{\sum L_{\rm i} u_{\rm i}^2}{\sum \sum_{\rm j<i} L_{\rm i} L_{\rm j} |\boldsymbol{R}_{\rm i} - \boldsymbol{R}_{\rm j}|^{-1}} \tag{78}$$

where $|\boldsymbol{R}_{\rm i} - \boldsymbol{R}_{\rm j}|$ is the projection of $|\boldsymbol{r}_{\rm i} - \boldsymbol{r}_{\rm j}|$ on the plane of the sky.

However this measure should be used only if N is large, or otherwise statistically, ie, averaged over a large number of groups to find the $\langle M/L \rangle$ of the ensemble. Note that this estimator is very sensitive to the group-finding algorithm, selection procedure, selection function corrections (ie., corrections to take into account the fact that the galaxy density artificially decreases with depth in magnitude/flux limited samples). Furthermore, projection effects (ie; inclusion in the group of a foreground or background galaxy) is also a source of error. For example the inclusion of a non-member would result in an artificially higher M/L while conversely the exclusion of a member (due to a high $u_{\rm i}$) would underestimate the M/L.

The mass-to-light ratio for groups of galaxies (cf. [132]) is:

$$M/L \sim 180 \pm 50 M_{\odot}/L_{\odot} \ . \tag{79}$$

Clusters of Galaxies: The most common approach to measure the cluster M/L is based on the assumption that clusters are in virial equilibrium, for which we do have strong indications. The first step in determining M/L is to measure the cluster velocity dispersion accurately. Using the recent compilation of 395 $R \geq 0$ ABELL/ACO cluster velocity dispersions [167] I find:

$$\sigma \equiv \langle (v - \bar{v})^2 \rangle^{1/2} \approx 750 \pm 322 \ {\rm km/sec}$$

However, this value is based even on clusters for which the velocity dispersion was determined from a very small number of galaxy redshifts, a fact which increases the possibility of assigning an erroneous σ-value. This can be seen in the left panel of Fig.11 were we plot the normalized σ frequency distribution for clusters with $N_{\rm z} < 20$ and $N_{\rm z} > 20$. The skewed distribution to large σ-values for $N_{\rm z} < 20$ is evident, while the mean σ-value is smaller than for the $N_{\rm z} > 20$ case. As a compromise between having enough redshifts per cluster, in order to get a reliable σ-value, and a large cluster sample, we choose those with $N_{\rm z} > 20$. For these 195 clusters I find that:

$$\sigma \approx 822 \pm 294 \ {\rm km/sec} \ .$$

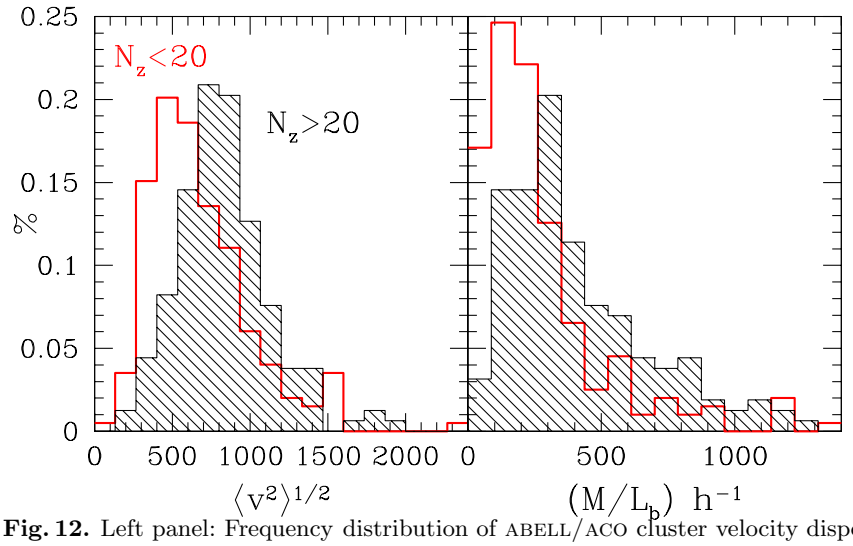

Fig. 12. Left panel: Frequency distribution of ABELL/ACO cluster velocity dispersions based on $N_z < 20$ (empty histogram) and on $N_z > 20$ (shaded histogram). Right panel: The corresponding M/L distribution.

A consistent value of $\sigma \simeq 940 \pm 208$ km/sec has been found from the 16 high-redshift clusters of the CNOC project [32] and a variety of methods used to define cluster membership and account for interlopers [23].

Now from the Virial theorem, $M = 2\sigma^2 r_a/G$, we have:

$$M_{\rm c}(\leq r_{\rm a}) \approx 7 \times 10^{14} \left(\frac{\sigma}{1000}\right)^2 h^{-1}\, M_\odot\ . \tag{80}$$

where $r_{\rm a} = 1.5\, h^{-1}$ Mpc. Using a number-galaxy weighted luminosity estimation, and assuming an average cluster value in the optical of $L \simeq 10^{12}\, h^{-2}\, L_\odot$ (cf. [4]), we obtain the distribution of M/L values (see right panel of Fig.11). Since the distribution is non-Gaussian we quote below the median and 68% confidence levels:

$$(M/L)_{\rm c} \approx 320^{+170}_{-85}\, h\, M_\odot/L_\odot \tag{81}$$

A more accurate method that can be used to estimate cluster mass is based on the measurements of the X-ray emission from the ICM gas, similar to the method used for individual elliptical galaxies (76). Although not strictly correct, usually an isothermal cluster profile is used ($\mathrm{d}\ln T/\mathrm{d}\ln r = 0$), which greatly simplifies calculations. However, recent experiments have shown that indeed the cluster Temperature does not vary significantly with radius ($\mathrm{d}\ln T/\mathrm{d}\ln r \simeq -0.7 \sim -0.8$). Estimates of M/L derived with this method are in general agreement with (81).

Table 2. Mass-to-light ratios and contribution to $\Omega_{\rm m}$ for the different scales.

Object	scale (h^{-1} Mpc)	$\langle M/L\rangle\ h^{-1}$	$\Omega_{\rm m}$
Spirals	0.02	10 ± 2	0.0071 ± 0.0015
Ellipticals	0.02	25 ± 5	0.018 ± 0.004
Galaxy pairs	0.1	80 ± 20	0.057 ± 0.012
Groups	0.8	180 ± 60	0.13 ± 0.09
Clusters	1.5	320^{+170}_{-85}	$0.23^{+0.12}_{-0.06}$

Global luminosity density and $\Omega_{\rm m}$: We estimate the value of $\langle L\rangle$ using the galaxy luminosity function which is defined such that $\Phi(L)dL$ is the number density of galaxies having total luminosity in the interval $(L, L+dL)$. A good fit to the observed luminosity function of the field population of galaxies is provided by the *Schechter* function [153]:

$$\Phi(L) = \frac{\phi_*}{L_*}\left(\frac{L}{L_*}\right)^{\alpha} \exp\left[-L/L_*\right] \tag{82}$$

where $\alpha = -1.29 \pm 0.11$, $\phi_* = 1.3 \pm 0.3 \times 10^{-2} h^3$ Mpc^{-3} and $L_* = 1.1 \times 10^{10} h^{-2} L_\odot$ (see also [52]). Then the mean luminosity density, corresponding to (82), is:

$$\langle L\rangle = \int L\Phi(L)dL = \phi_* L_* \Gamma(\alpha+2) \approx 2 \times 10^8 h L_\odot \ {\rm Mpc}^{-3} \tag{83}$$

Using the value of $\rho_{\rm cr}$ (15) we have:

$$\frac{M}{L} = \frac{\rho_\circ}{\langle L\rangle} = \frac{\Omega_{\rm m}\rho_{\rm cr}}{\langle L\rangle} \simeq 1400\ \Omega_{\rm m}\ h\ M_\odot/L_\odot\ . \tag{84}$$

In Table 2 we summarize the $\langle M/L\rangle$ values found at different scales and the corresponding contribution to $\Omega_{\rm m}$.

Since galaxy clusters are the deepest potential wells in the Universe and they accumulate baryonic and DM from large volumes, it is expected that their M/L ratio could represent the Universal value. This view is supported by the fact that the increasing trend of M/L with scale (seen in Table 2) reaches a plateau at the corresponding value of the clusters (cf. [3], [6]). Therefore the universal value, as given by the clusters is:

$$\Omega_{\rm m} \simeq 0.23^{+0.12}_{-0.06}$$

The analysis of the CNOC sample of 16 distant clusters ($0.17 < z < 0.55$), provides a consistent value but with significantly smaller uncertainty; $\Omega_{\rm m} \simeq 0.19 \pm 0.06$ (see [32] and references therein).

3.5 Cluster Baryon Fraction:

Assuming that on the scales from which clusters accrete matter during their formation, there is no segregation of baryons and DM, then the ratio of baryonic

to total matter in clusters is representative of the universal value $(\Omega_{\rm B}/\Omega_{\rm m})$, something supported also by hydro-dynamical numerical simulations. Galaxies add up to only $\sim 5\%$ of the total cluster mass, while the hot gas, which fills the space between galaxies, accounts for $\sim 20\%$.

So adding up the galactic and gas contribution to the mass of the cluster we obtain a measure of the total baryonic cluster mass, $M_{\rm B}$ and then if we can measure the total mass of the cluster, $M_{\rm tot}$, we can estimate $\Omega_{\rm m}$.

Assuming hydrostatic equilibrium, the gas traces the cluster total mass, and using (76) we can obtain, $M_{\rm to}$. Most studies (cf. [186] [103] [58]) find:

$$\frac{\Omega_{\rm B}}{\Omega_{\rm m}} = \frac{M_{\rm B}}{M_{\rm tot}} \simeq 0.10 - 0.13 \quad \text{for } h = 0.72 \tag{85}$$

From the primordial nucleosynthesis constraints (see 63) and from the recent Bommerang results we have that $\Omega_{\rm B}h^2 \simeq 0.020 \pm 0.004)$, which for $h = 0.72$ gives $\Omega_{\rm B} \simeq 0.04$ and therefore:

$$\Omega_{\rm m} \simeq 0.35\ (\pm 0.05)$$

Note however that in a recent study [147], the application of various corrections to account for the clumping of gas and the gas fraction gradients, within the virial radius of a cluster, resulted in significantly lower values of the baryon fraction and thus higher values of $\Omega_{\rm m}$.

3.6 Large-Scale Velocity Field:

As already discussed in section 2, the local gravitational field produces peculiar velocities superimposed on the general expansion (35). Measurements of peculiar velocities can provide direct information on the mass content of the Universe, since they can be related to the density fluctuation field, which itself can be observed directly. The basic idea is that a body of mass M will produce a different gravitational field if it is embedded in a low or high density Universe. In a high density Universe it will correspond to a lower density fluctuation than in a low density Universe and thus it will produce weaker/stronger gravitational effects, respectively.

If $\delta(\boldsymbol{x}) = (\rho(\boldsymbol{x}) - \bar{\rho})/\bar{\rho}$ is the mass fluctuation at $\boldsymbol{x}$ then using linear perturbation theory, continuity, Euler and Poisson equations, we obtain the that the growing mode of the evolution of fluctuations is:

$$\delta \propto D(t) \Longrightarrow \frac{\dot{\delta}}{\delta} = \frac{\dot{D}}{D}$$

Note that in the EdS universe we have $D(t) = t^{\frac{2}{3}}$. Linearizing the mass continuity equation, we obtain:

$$\boldsymbol{\nabla}\cdot\boldsymbol{v} = -R\dot{\delta} = R\delta\frac{\dot{D}}{D} \tag{86}$$

which has solution:

$$\boldsymbol{v}(\boldsymbol{x}) = \frac{\Omega_{\rm m}^{0.6}}{4\pi b} \int \frac{\boldsymbol{x}-\boldsymbol{x'}}{|\boldsymbol{x}-\boldsymbol{x'}|^3}\, \delta_{\rm tr}(\boldsymbol{x})\, {\rm d}^3x \equiv \frac{\Omega_{\rm m}^{0.6}}{b}\boldsymbol{D}(\boldsymbol{x}) \tag{87}$$

where the the dipole vector $D(x)$ is related to the gravitational acceleration vector and b is the bias factor relating the mass-tracer fluctuations ($\delta_{\rm tr}$) with the underline mass fluctuation field (72). Note that in most cases it is expected that $b > 1$, ie., the *tracer* distribution is more clustered than the matter. This has been born out from the study of random Gaussian fields in which the higher the density fluctuations the more clustered they are (cf. [8]) and from the correlation function analysis of extragalactic objects by which it was found that the *relative* bias factor of ABELL clusters, optical and IRAS galaxies is $[b_{\rm cl} : b_{\rm op} : b_{\rm IR} = 4.5 : 1.3 : 1]$ (see [111]). It is therefore expected that this hierarchy of decreasing correlations should continue to the underlying mass distribution. Note that (87) can be written as [114]:

$$\boldsymbol{v} = \frac{2}{3}\frac{\boldsymbol{g}}{H_\circ \Omega_{\rm m}^{0.4}} \tag{88}$$

One then needs good estimates of peculiar velocities, knowledge of the matter tracer fluctuation field to estimate $D(x)$, and an understanding of the biasing between matter and light in order to put constraints on $\Omega_{\rm m}$.

Local Group Dipole: The above test was first applied to the Local Group, since from the CMB dipole we have an excellent measurement of its peculiar velocity. The dipole moment, $D(x)$, is measured using different populations of extragalactic objects (IRAS, optical galaxies, AGN's, ABELL/ACO optical or X-ray clusters), weighting each object by r^{-2} or by a weight proportional to r^{-2} (like flux, diameter^2). Under the assumption that light traces the mass, then the dipole moment is a measure of the peculiar force acting on the LG.

In linear theory the peculiar velocity is parallel to the acceleration and therefore finding an approximate alignment of the two vectors tells us that the fluctuations causing this motion are present within the depths of the sample, provided that the dipole moment converges to its final value before the characteristic depth of the sample. Furthermore, it tells us that possible local non-linear effects do not strongly affect the $\boldsymbol{D}(x)$ determination.

The multipole components of some mass-tracer distribution are calculated by summing moments. For example the monopole and dipole terms are: $M = 1/4\pi \sum w_{\rm i}$ and $\boldsymbol{D} = 3/4\pi \sum w_{\rm i}\boldsymbol{r}_{\rm i}$ where $w_{\rm i} \propto r^{-2}$. The dipole vector, $\boldsymbol{D}$, is calculated by weighting the unit directional vector pointing to the position of each galaxy, with the weight $w_{\rm i}$, of that galaxy and summing over all N available galaxies in the survey. Note however, that even a uniform distribution would produce a dipole, the so-called shot-noise dipole, if it is sparsely sampled. The shot noise error is $\langle \boldsymbol{D}\cdot\boldsymbol{D}\rangle^{\frac{1}{2}} = 3/4\pi\ N^{\frac{1}{2}}\langle w^2\rangle^{\frac{1}{2}}$, and even in a clustered distribution, the estimated dipole will always have such a shot-noise contribution which should be taken into account. A further difficulty is that whole-sky distributions of extragalactic mass-tracers are unavailable, either due to survey

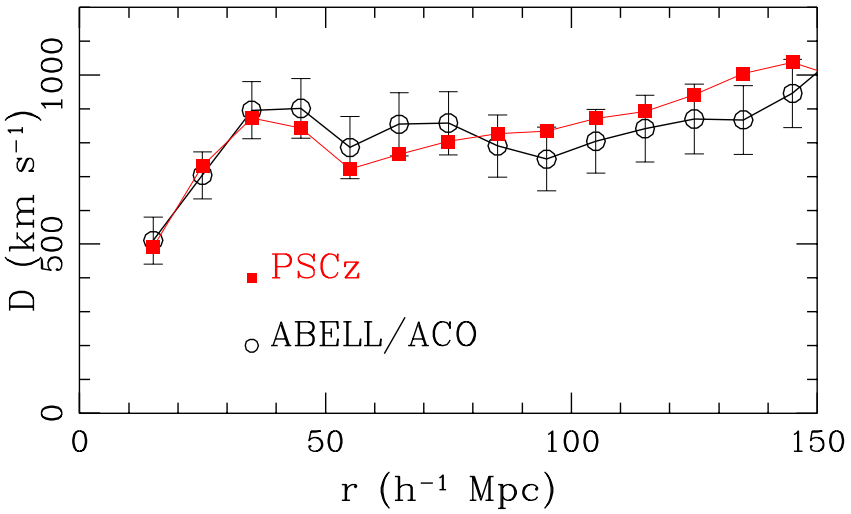

Fig. 13. Dipole amplitude build up as a function of distance of the IRAS PSCZ galaxy and the ABELL/ACO cluster samples. The ABELL/ACO cluster dipole has been scaled down by a factor of ~ 4, to take into account the relative bias factor (from [124]).

limitations, extinction near the Galactic plane, cirrus emission, magnitude, flux or diameter limits (which will cause a different population mix to be sampled at different depths, and the contributions of the 'faint' or 'small' objects to be missed). Therefore, complicated corrections should be applied, which usually have well understood properties and in any case are always tested with numerical or Monte-Carlo simulations.

Results from many different galaxy catalogues (optical or IR) tracing depths up to $\sim 100 - 120\, h^{-1}$ Mpc, show dipoles that are well aligned with the CMB dipole (mass dipole) which indicates that galaxies trace the mass distribution. Some recent analysis of IRAS galaxies provide values:

$$\Omega_{\rm m} \approx 0.62(\pm 0.13)\, b_{\rm IR}^{1.66}$$

(cf. [166], [145] and references therein) and

$$\Omega_{\rm m} \approx 0.55(\pm 0.2)\, b_{\rm op}^{1.66}$$

(cf. [73]). The difference between the above values is most probably due to the different biasing factors ie., $b_{\rm IR} < b_{\rm op}$, which is natural since optical galaxies trace more accurately the deep potential wells (clusters) while the IRAS galaxies trace better the field. In fact it has been found that $b_{\rm op}/b_{\rm IR} \simeq 1.2 - 1.4$ (cf. [111] [7] [124] and references therein). Furthermore, if IR galaxies are biased with respect to mass (ie., if $b_{\rm IR} \gtrsim 1.2$) then the above results could imply: $\Omega_{\rm m} \simeq 1$.

Now, *galaxy clusters*, being the largest gravitationally-collapsed structures in the universe and luminous enough to be detected to very large distances, have also been used to probe the local acceleration field. Most studies are based on the optically selected ABELL/ACO clusters [1] and they provide strong evidence that the LG dipole has significant contributions from depths up to $\sim 160h^{-1}$ Mpc (see Fig.12 and [152], [122], [26]). However, due to the the volume incompleteness of richness class R=0 clusters (cf. [110]) and to optical projection effects (enhancement of galaxy density along the direction of foreground rich clusters which cause inherently poor background clusters or groups to appear rich enough to be included in the sample), these results had to be checked. Using well defined X-ray cluster samples free of the above effects [51] indeed the results were verified [123]. The results based on optical or X-ray clusters, imply:

$$\Omega_{\rm m} \approx 0.07 - 0.09\, b_{\rm cl}^{1.66}$$

Note that from the correlation function analysis of ABELL/ACO clusters [111] we have that the relative bias factor between clusters and IRAS galaxies is around $b_{\rm cl,IR} \simeq 4.5$ and if the bias factor of IRAS galaxies with respect to the mass is $b_{\rm g} \geq 1$, then the above results are consistent with $\Omega_{\rm m} \simeq 1$.

It is extremely interesting that the galaxy distribution in the local universe (within $\sim 100\ h^{-1}$ Mpc) produces a gravitational acceleration that is aligned with that produced by the matter distribution (as determined by the CMB dipole) and in the same time the distribution of clusters of galaxies on larger scales $R \lesssim 250\ h^{-1}$ Mpc produce also a gravitational acceleration aligned with that of the matter distribution. Furthermore the galaxy and cluster distributions produce Local Group acceleration profiles that are directly proportional to each other (see Fig.13), while the dipole in equal volume shells, seems to be roughly aligned with the CMB dipole direction out to very large depths (cf. [122], [11]). This implies that there is a coherent anisotropy in the mass distribution over a region with a diameter of $\sim 300\ h^{-1}$ Mpc, which then sets a lower limit to the scales over which the Cosmological Principle applies.

However, there is a dichotomy among different studies trying to identify the convergence scale of the dipole, or equivalently what is the largest scale over which we observe bulk motions. The previously discussed dipole studies as well as some peculiar velocity studies (cf. [89], [75], [188]), support the view of a large convergence depth (radius of $\sim 150\ h^{-1}$ Mpc). Other peculiar velocity studies (cf. [38], [41], [40], [36], [39]) support a significantly smaller convergence depth $\sim 60\ h^{-1}$ Mpc.

POTENT - from Radial Velocities to Density Field: In the previous analysis only one velocity was used, that of the Local Group, and although it is very well measured we still have the problem of cosmic variance. Therefore, ideally the velocity-acceleration comparison should be performed for a number of "observers". This has been possible due to the POTENT algorithm proposed in [14] and developed extensively by Dekel and his collaborators (cf. [46] and references therein).

Fig. 14. (Included separately as a JPG image) Comparison of predicted density and velocity fields: Left panel shows the observed ABELL/ACO density field and the corresponding predicted velocity field. Right panel shows the matter density field predicted by POTENT and the peculiar velocity field of Mark III galaxies (from [27]).

The basic idea follows. The large-scale velocity field, evolving via gravitational instability, is expected to be irrotational $\boldsymbol{\nabla}\times\boldsymbol{v}=0$. This remains a good approximation in the mildly-nonlinear regime as long as the field is properly smoothed. This implies that the velocity field can be derived from a scalar potential,

$$\boldsymbol{v}(\boldsymbol{x}) = -\boldsymbol{\nabla}\Phi(\boldsymbol{x}) \,,$$

and thus the potential can in principle be computed by integration along the lines of sight,

$$\Phi(\boldsymbol{x}) = -\int_0^r u(r',\theta,\phi)\mathrm{d}r' \,. \tag{89}$$

The two missing transverse velocity components are then recovered by differentiation. Then from (86) we recover the density fluctuation field, which can then be compared to the observed density field, determined from large whole-sky surveys. The current sampling of galaxies enables reliable dynamical analysis, with a smoothing radius as small as $\sim 10\,h^{-1}$Mpc, where $|\boldsymbol{\nabla}\cdot\boldsymbol{v}|$ obtains values larger than unity and therefore mildly non-linear effects play some role.

The most reliable density-density analysis, incorporating certain mildly nonlinear corrections, is the comparison of the IRAS 1.2 Jy redshift survey and the Mark III catalogue of peculiar velocities yielding, at Gaussian smoothing of $12\,h^{-1}$Mpc [158]:

$$\Omega_{\rm m} \simeq 0.82(\pm 0.16)\, b_{\rm IR}^{1.66}$$

A similar analysis, using optical galaxies [74] has provided a somewhat lower value:

$$\Omega_{\rm m} \simeq 0.6\ (\pm 0.15)\, b_{\rm op}^{1.66}$$

in accordance with the expected higher biasing parameter of optical galaxies with respect to IRAS ones. These results are consistent with the dipole analyses and with $\Omega_{\rm m}\simeq 1$ for $b_{\rm IR}\gtrsim 1.2$.

However, a variety of methods using v-v comparisons (eg. VELMOD - [187]), developed to compare observed and derived velocities (using either the IRAS or ORS gravity fields), typically yield values of: (cf. [189] and references therein, [28], [18]):

$$\Omega_{\rm m} \simeq 0.3\ (\pm 0.1)\, b_{\rm IR}^{1.66}$$

$$\Omega_{\rm m} \simeq 0.14\ (\pm 0.05)\, b_{\rm op}^{1.66}$$

which are consistent with $\Omega_{\rm m}<1$ for any reasonable value of $b_{\rm g}$. Therefore, there seems to be a discrepancy between different analyses, even if in some cases, they use the same data, a fact that needs further study and tests of the reliability of each method.

A study [27] using the ABELL/ACO clusters to trace the density field and comparing it with the POTENT reconstructed field from the Mark III catalogue of peculiar velocities (see Fig.14) found:

$$\Omega_{\rm m} \approx 0.07 - 0.09\, b_{\rm cl}^{1.66}$$

in good agreement with the dipole analysis of ABELL/ACO clusters and consistent with $\Omega_{\rm m} \simeq 1$ for the estimated value of $b_{\rm cl}$ [111].

Local Group infall to Virgo: This is an interesting method to calculate $\Omega_{\rm m}$ on scales of $\sim 10\ h^{-1}$ Mpc. One relates the Local Group infall (towards the centre of the Local supercluster) velocity with the acceleration induced to the LG by the mass overdensity in the Local Supercluster, assuming a point-mass approximation. We have from (87):

$$\boldsymbol{v}_{\rm in} = \frac{2}{3}\frac{\boldsymbol{g}}{H_\circ \Omega_{\rm m}^{0.4}} = \frac{2}{3}\frac{G\delta M}{H_\circ \Omega_{\rm m}^{0.4} r^2} \tag{90}$$

From (72) we have that the galaxy fluctuations is a biased tracer of the underline mass fluctuation field:

$$b\frac{\delta M}{M} \simeq \delta_{\rm g} \Longrightarrow \delta M \simeq \frac{M\delta_{\rm g}}{b}\ . \tag{91}$$

Thus from (90) we have:,

$$v_{\rm in} = \frac{1}{3}\frac{\Omega_{\rm m}^{0.6}}{b}\ cz\ \delta_{\rm g}(1+\delta_{\rm g})^{-1/4}$$

where the mildly non-linear correction on the right-hand side is according to [191]. A recent study [174] using the SBF method to determine the local velocity field within $cz \lesssim 3000$ km/sec find a Virgo-centric infall of $v_{\rm in} \sim 140$ km/sec in agreement with ~ 160 km/sec, implied from the Virgo contribution to the X-ray cluster dipole [123]. Furthermore we have that $cz \simeq 1005$ km/sec [104] [149] and $\delta_{\rm g} \simeq 2.8 \pm 0.5$. Therefore we obtain:

$$\Omega_{\rm m} \simeq 0.1(\pm 0.02)\ \left(\frac{v_{\rm in}}{150\ {\rm km/sec}}\right)^{1.66} b_{\rm op}^{1.66}$$

Although this method of determining $\Omega_{\rm m}$ is 'clean', the fact that the local peculiar velocity field is affected by mass concentrations well beyond the Local supercluster introduces a further uncertainty in the determination of $\Omega_{\rm m}$.

Velocity-Field results: The outcome of the different large-scale dynamical studies do not converge to a unique value of the mass density parameter. There is need to check the methods and understand the source of this discrepancy. In Table 3 I sum up the different results from the different velocity-field analyses.

Table 3. Results from some recent velocity field studies

Type of study	$\Omega_{\rm m}\, b_{\rm IR}^{-1.66}$	$\Omega_{\rm m}\, b_{\rm op}^{-1.66}$	$\Omega_{\rm m}\, b_{\rm cl}^{-1.66}$
Dipole	0.62	0.55	0.08
POTENT/Mark III	0.82	0.6	0.08
VELMOD	0.3	0.14	
LG-infall		0.1	

3.7 Rate of Cluster Formation Evolution:

The rate of growth of perturbations is different in universes with different matter content. For example, the perturbation growth in a $\Omega_{\rm m} = 1$ universe is proportional to the scale factor, ie., $\delta \propto (1+z)^{-1}$, while in the extreme case of an empty universe ($\Omega_m = 0$); δ = constant. From (32) we see that $\Omega_{\rm m} < 1$ universes will behave dynamically as an $\Omega = 1$ universe at large enough redshift, and at some redshift $z \sim 1$ curvature dominates and perturbations stop evolving and freeze, allowing clusters to relax up to the present epoch much more than in an $\Omega_{\rm m} = 1$ model, in which clusters are still forming. This can be seen clearly in Fig.15 where we plot the evolution of the perturbation growth factor, defined as:

$$f = \frac{{\rm d}\ln\delta}{{\rm d}\ln R}\,.$$

For a $\Omega_\Lambda = 0$ universe, $f \simeq \Omega_{\rm m}^{0.6}$ (cf. [115]) and thus for the EdS model $f = 1$. For $\Omega_\Lambda > 0$ models there is a redshift dependence of f, but in the present epoch it is indistinguishable from the corresponding value of the open ($\Omega_{\rm m} = 1 - \Omega_\Lambda$) model [86]. It is evident that an $0 < \Omega_\Lambda < 1$ universe behaves as an $\Omega_{\rm m} = 1$ model up to a lower redshift than the corresponding open model, while at redshifts $z \lesssim 1$ it behaves like an open model, which implies that clusters should be dynamically older in such a model than in the EdS. Therefore one should be able to put constraints on Ω from the evolution of various indicators of cluster formation, especially in the range where the dynamical evolution between the models differs maximally (vertical dashed lines in Fig.15).

Ideally, one would like to study the evolution of the cluster mass function but since light is what we observe (temperature as well - due to the hot ICM X-ray emission), various related indicators are usually studied (Luminosity function, temperature function, morphology etc), but then one has to pass through the machinery provided by the Press-Schechter formalism [128], which gives the mass function of collapsed halos at any epoch as a function of the cosmological parameters that enter through the assumed power spectrum of perturbations.

Luminosity function: Based mostly on EINSTEIN and ROSAT surveys, many studies have found an evolving X-ray luminosity function, ie., less $z \gtrsim 0.3$ clusters than expected for a no-evolving luminosity function, ie., a negative evolution (cf. [63] and references therein). Such a behaviour is expected in models with

$$\Omega_{\rm m} \simeq 1$$

However, see [69] for a different view.

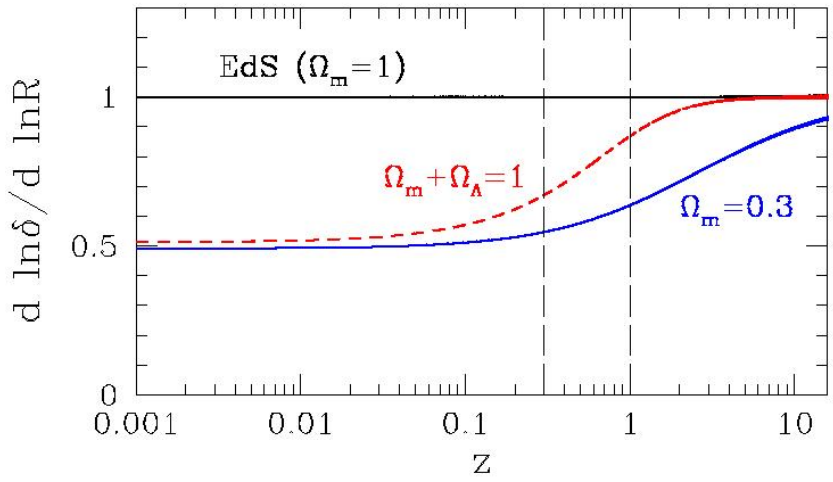

Fig. 15. The evolution of the perturbation growth factor, f, in 3 models (EdS, open $\Omega_{\rm m} = 0.3$ and the currently popular flat $\Omega_\Lambda = 0.7$). The vertical dashed lines indicate the redshift range $0.3 \lesssim z \lesssim 1$ where the 3 models, jointly, differ maximally.

Temperature function: Estimates of the temperature of the X-ray emitting ICM gas can be reliably estimated from the iron line-emission. Then the cluster temperature can be either transformed to a mass (assuming hydrostatic equilibrium and isothermality) and thus derive a mass function to compare with the Press-Schechter predictions (cf. [133] and references therein) pointing to $\Omega_{\rm m} < 0.3$, or use the evolution of the temperature distribution function. Again different studies find either no evolution (cf. [56], [68]) pointing to

$$\Omega_{\rm m} \simeq 0.3 - 0.5$$

or evidence for evolution [180] [19] pointing to

$$\Omega_{\rm m} \simeq 0.7 - 1$$

Evolution of $L - T$ relation: Under the assumption of hydrostatic equilibrium and isothermality one can easily show, from Euler's equation, that the bremsstrahlung radiation temperature is $T \propto M_{\rm v}/R_{\rm v}$ (where $M_{\rm v}$ and $R_{\rm v}$ are the cluster virial mass and radius). Using the spherical collapse top-hat model [114] one obtains $R_{\rm v} \propto T^{1/2}\, \Delta(z)^{-1/2}\, E(z)^{-1/2}$, and then by using (56):

$$L_{\rm x} \propto f_{\rm g}^2 M_{\rm v}^2 T^{1/2} R_{\rm v}^{-3} \tag{92}$$

where $f_{\rm g}$ is the gas mass fraction. Then one finds (cf. [31]):

$$L_{\rm x} \propto f_{\rm g}^2\, T^2\, \Delta(z)^{1/2}\, E(z)^{1/2}$$

where $E(z)$ is given by (18) and $\Delta(z)$ is the ratio of the average density within the virialized cluster ($\lesssim R_{\rm v}$) and the critical density at redshift z, which also depends on the cosmological model. However, this model fails to account for observations which show a steeper T-dependence, $L_{\rm x} \propto T^{3-3.3}$ (such a dependence can be recovered from (92) if $f_{\rm g} \propto T^{1/2}$). In any case, the $L-T$ relation is expected to evolve with time in a model dependent way. Most studies (see references in [155]) have found *no* evolution of the relation while a recent study of a deep ($z \sim 0.85$) ROSAT cluster survey [25] found:

$$\Omega_{\rm m} \sim 0.35$$

However, there are many physical mechanisms that affect this relation (eg. gas cooling, supernova feedback etc) and in ways which are not fully understood (cf. [66]).

Evolution of Cluster Morphology: As we have already discussed, in an open or a flat with vacuum-energy contribution universe it is expected that clusters should appear more relaxed with weak or no indications of substructure. Instead, in a critical density model, such systems continue to form even today and should appear to be dynamically active (cf. [134], [59], [85]). Using the above theoretical expectations as a cosmological tool is hampered by two facts (a) *Ambiguity in identifying cluster substructure* (due to projection effects) and (b) *Post-merging relaxation time uncertainty* (cf. [150]). However, criteria of recent merging could be used to identify the rate of cluster morphology evolution and thus put constraints on $\Omega_{\rm m}$. Such criteria have been born out of numerical simulations (cf. [139], [140]) and are based on the use of multiwavelength data, especially optical and X-ray data but radio as well (cf. [192], [154]). The criteria are based on the fact that gas is collisional while galaxies are not and therefore during the merger of two clumps, containing galaxies and gas, we expect: (*1*) a difference in the spatial positions of the highest peak in the galaxy and gas distribution, (*2*) due to compression, the X-ray emitting gas to be elongated perpendicularly to the merging direction, and (*3*) temperature gradients to develop due to the compression and subsequent shock heating of the gas. The first two indicators are expected to decay within ~ 1 Gyr after the merger, while the last may survive for a considerably longer period (see for example Fig.16). For such a study to be fruitful, a large number of clusters, ideally covering the redshift range $0.3 \lesssim x \lesssim 1$, must be imaged in both the optical and X-ray band.

However, a rather cruder but still useful test of cluster morphological evolution could be used. For example, cluster ellipticity is a relatively well defined quantity; although systematic effects due to projections in the optical or the strong central concentration of the X-ray emitting gas (since $L_{\rm x} \propto n_{\rm e}^2$), should be taken into account (cf. [81]). An early study, using the Lick map [121], had found that cluster ellipticity decreases with redshift, however due to possible systematic effects involved in the construction of the data, they did not attach any weight to this discovery. Recently, two studies using optical and/or X-ray data [100] [127] (see also [120]) found that indeed the cluster ellipticity decreases with

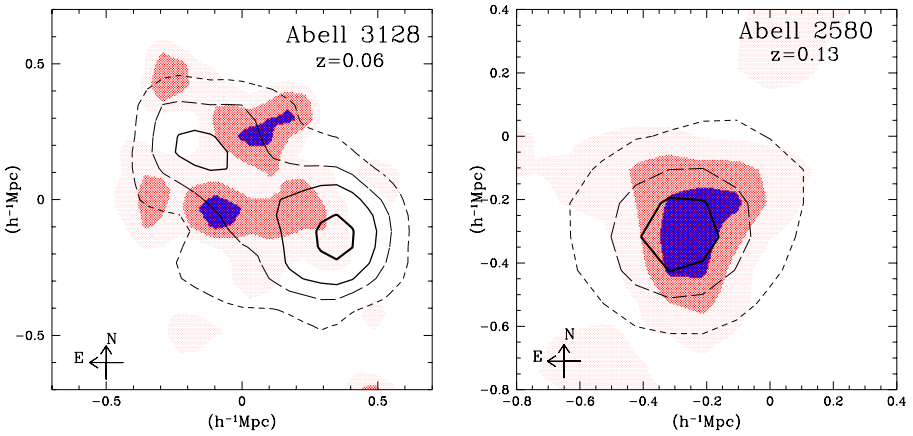

Fig. 16. Optical APM (colour) and ROSAT X-ray (contour) images of 2 ABELL clusters. Peaks of the APM galaxy distribution is shown in blue. A3128 has the signature of a recent merger: the peaks in the distribution of galaxies and in X-ray emitting gas are orthogonal to each other. A2580 on the other side seems a smooth relaxed cluster with the gas and galaxies tracing the cluster potential (from [120]).

redshift in the recent past, $z \lesssim 0.15$ (see Fig.17) This was interpreted by [100] as an indication of a low-$\Omega_{\rm m}$ universe because in such a universe one expects that merging and anisotropic accretion of matter along filaments will have stopped long ago. Thus the clusters should be relatively isolated and gravitational relaxation will tend to isotropize the clusters reducing their ellipticity, more so in the recent times.

If this is the case then one should expect an evolution of the temperature of the X-ray emitting gas as well as the X-ray cluster luminosity which should follow the same trend as the cluster ellipticity, decreasing at recent times, since the violent merging events, at relatively higher redshifts, will compress and shock heat the diffuse ICM gas [138]. Such evidence was presented in [127] using a compilation of measured ICM temperatures and luminosities in two volume limited X-ray cluster samples (based on the XBAC and BCS samples). Also, one could naively expect an evolution of the cluster velocity dispersion, increasing at lower redshifts, since virialization will tend to increase the cluster 'thermal' velocity dispersion. In [65] no evolution was found between a local sample ($z \lesssim 0.15$) and a distant one $0.15 \lesssim z \lesssim 0.9$. However, unrelaxed clusters can also show up as having a high velocity dispersion due to either possible large peculiar velocities of the different sub-clumps [142] or due to the possible sub-clump virialized nature. Therefore, a better physical understanding of the merging history of clusters is necessary in order to be able to utilize the velocity dispersion measure as an evolution criterion.

Other related studies, using the morphological characteristics of the large-scale structures, have been used to place cosmological constraints. For example, the shapes of superclusters and voids, using the IRAS-PSCZ redshift survey and

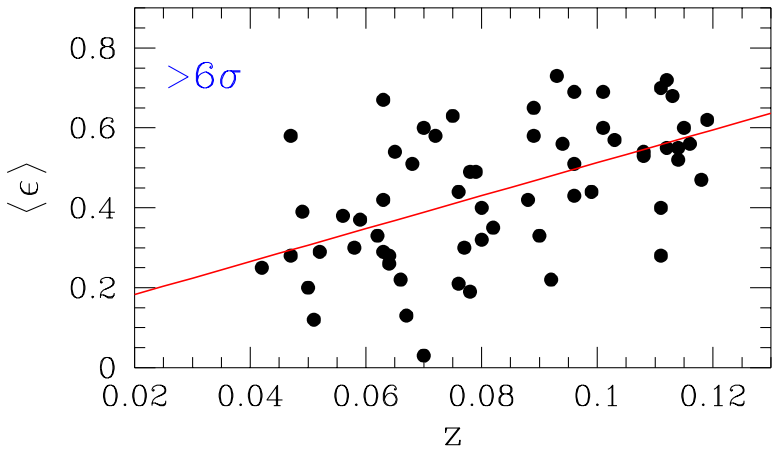

Fig. 17. The evolution of ellipticity in APM clusters with significant substructure [120]

the ABELL/ACO cluster distribution show a clear preference for a Λ-CDM model over a $\Omega_{\rm m} = 1$ model [13] [126] [82] [102] but see [2].

4 Summary

I have attempted to present the basic ideas behind many (but not all) of the current methods used to estimate various Cosmological parameters, especially the Hubble constant ($H_\circ$), the curvature of the Universe (Ω) and its matter content ($\Omega_{\rm m}$). To do so I reviewed some basics of the standard, Robertson-Walker, Cosmology in order to highlight the interrelations of the Cosmological parameters and the way they affect the global dynamics of the Universe.

The results of a variety of different analyses, based on a multitude of data, point towards a *concordance* model, which is a flat, $\Omega_\Lambda \simeq 0.7$, with an inflationary spectral index $n \simeq 1$, $h \simeq 0.72$, $\Omega_{\rm B} \simeq 0.04$, $t_\circ \simeq 1.31$ Gyr's. Nevertheless there are conceptual problems and open issues that may or may not prove to be daunting.

For example, the $\Omega_\Lambda = 0.7$, $h = 0.7$ model seems to have problems generating the correct power on galactic scales. Detailed numerical simulations of [80] show that this model has much more power on small scales to be reconciled with observations (see discussion in [129]). Furthermore, there is the fine tuning problem. Why does the energy density of the vacuum have a value like: $\Omega_\Lambda \sim \Omega_{\rm m} \sim 1$, implying that it dominates the Universe just NOW! An easy way out would be to invoke *anthropic* arguments [10], but it is too feeble a justification, especially since the different contributions to Λ at the early phase transitions are 50 - 100 orders of magnitude larger than what is observed. One would have to invoke a fine-tuning in order for the different contributions to cancel out, but yet not completely! However, theoretical models are being developed in an attempt to alleviate such problems (cf. [57]), some by allowing Λ to be a function of time (see [148] and references therein).

Acknowledgments

I would like to thank Spiros Cotsakis and Lefteris Papandonopulos for organizing this wonderful school and for their hospitality in the island of Pythagoras. I would also like to thank the students of the school for their interest, their stimulating discussions and their ...dancing abilities. Many thanks to Ed Chapin that had the patience to go through the text and correct my "Greekisms".

References

1. Abell, G.O. 1958, ApJ Suppl., 3, 211
   Abell, G.O., Corwin Jr, H.G. & Olowin, R.P., 1989, ApJ Suppl., 70, 1
2. Arbabi-Bidgoli, S., Mueller, V., 2002, MNRAS, in press, *astro-ph/0111581*
3. Bahcall, N.A., Lubin, L.M., Dorman, V., 1995, ApJ, 447, L81
4. Bahcall, N.A., 1999, in *Formation of Structure in the Universe*, Eds. Dekel & Ostriker, p.135, Camb. Univ. Press
5. Bahcall, N.A., 2000, Phys.Rep., 333, 233
6. Bahcall, N.A., Cen, R., Davé, R., Ostriker, J.P., Yu, Q., 2000, ApJ, 541, 1
7. Baker, J.E., Davis, M., Strauss, M.A., Lahav, O., Santiago, B.X., 1998, ApJ, 508, 6
8. Bardeen, J.M., Bond, J.R., Kaiser, N. & Szalay, A.S. 1986, ApJ , 304, 15
9. Barkhouse, W.A., Yee,H.K.C., Lopez-Cruz, O. 2002, in*Tracing Cosmic Evolution with Galaxy Clusters*, ASP Conference Series, in press
10. Barrow, J.D., Tipler, F.J., 1986, *The anthropic cosmological principle*, Oxford: Clarendon Press
11. Basilakos, S., Plionis, M., 1998, MNRAS, 299, 637
12. Basilakos, S., Plionis, M., Maddox, S., 2000, MNRAS, 316, 779
13. Basilakos, S., Plionis, M., Rowan-Robinson, M., 2001, MNRAS, 323, 47
14. Bertschinger, E., Dekel, A., 1989, ApJ, 336, L5
15. Binggeli, B. 1982, AA, 107, 338
16. Binnet, J., Merrifield, M., 1998, *Galactic Astronomy*, Princeton Univ. Press
17. Birkinshaw, M., 1999, Phys.Rep., 310, 97
18. Blakeslee, J.P., Davis, M., Tonry, J.L., Ajhar, E.A., Dressler, A., 2000, in the proceedings of the *Cosmic Flow* workshop, ASP Conf. series, Vol. 201, p.254, eds. S. Courteau & J.A. Willick
19. Blanchard, A., Sadat, R., Bartlett, J.G., Le Dour, M., 2000, AA, 362, 809
20. Blandford, R.D., Narayan, R., 1992 AARA, 30, 311
21. Bohringer, H., et al., 2001, AA, 369, 826
22. Borgani, S., 1995, Phys.Rep, 251, 1
23. Borgani, S., Girardi, M., Carlberg, R.G., Yee, H.K., Ellingson, E., 1999, ApJ, 527, 561
24. Borgani, S. & Guzzo, L., 2001, Nature, 409, 39
25. Borgani, S., et al., 2001, ApJ, 561, 13
26. Branchini, E., Plionis, M., 1996, ApJ, 460, 569
27. Branchini, E., Zehavi, I., Plionis, M., Dekel, A., 2000, MNRAS, 313, 491
28. Branchini, E., Freudling, W., Da Costa, L.N., Frenk, C.S., Giovanelli, R., Haynes, M.P., Salzer, J.J., Wegner, G., Zehavi, I., 2001, MNRAS, 326, 1191
29. Bridle, S.L., Zehavi, I., Dekel, A., Lahav, O., Hobson, M.P., Lasenby, A.N., 2001, MNRAS, 321, 333
30. Broom, V. & Clarke, C.J., 2002, ApJ, submitted, *astro-ph/0201066*
31. Bryan, G.L., Norman, M.L., 1998, ApJ, 495, 80
32. Carlberg, R.G., Yee, H.K.C & Ellingson, E., 1997, ApJ, 478, 462
33. Chiang, L.Y., Coles, P., 2000, MNRAS, 311, 809
34. Coles, P., 2001, in *Phase Transitions in the Early Universe: Theory and Observations*, Erice, Eds. H.J.de Vega, I.Khalatnikov, N.Sanchez.
35. Coles, P. & Lucchin, F., 1995, *Cosmology: the origin and evolution of cosmic structure*, John Wiley & Sons

36. Colless, M., Saglia, R.P., Burstein, D., Davies, R.L., McMahan, R.K., Wegner, G., 2000, in *Cosmic Flows Workshop*, ASP Conference Series, Vol. 201, p.54, Eds. S.Courteau & J. Willick
37. Colless, M., et al (2DFGRS TEAM), 2001, MNRAS, 328, 1039
38. Courteau, S, Willick, J.A., Strauss, M.A., Schlegel, D., Postman, M., 2000, ApJ, 544, 636
39. Da Costa, L.N., Bernardi, M., Alonso, M.V., Wegner, G., Willmer, C.N.A., Pellegrini, P.S., Maia, M.A.G., Zaroubi, S., 2000, ApJ, 537, 81
40. Dale, D.A., Giovanelli, R., Haynes, M.P.. Campusano, L.E., Hardy, E. Borgani, S., 1999, ApJ, 510, L11
41. Dale, D.A., Giovanelli, 2000, in *Cosmic Flows Workshop*, ASP Conference Series, Vol. 201., p.25, Eds. S.Courteau & J. Willick
42. Dalton G. B., Maddox S. J., Sutherland W. J., Efstathiou G., 1997, MNRAS, 289, 263
43. de Bernardis et al, 2002, ApJ, 564, 559
44. de Bernardis et al, 2000, Nature, 404, 955
45. de Grandi, S. & Molendi, S., 2002, ApJ, in press, *astro-ph/0110469*.
46. Dekel, A. 1999, in *Formation of Structure in the Universe*, Eds. Dekel & Ostriker, p.250, Camb. Univ. Press
47. Dodelson, S., et al (SSDS COLLABORATION), 2002, ApJ, in press, *astro-ph/0107421*
48. Dressler, A. 1980, ApJ, 236, 351
49. Dressler, A. 1981, ApJ, 243, 26
50. Dressler, A., Lynden-Bell, D., Burstein, D., Davies, R.L., Faber, S.M., Terlevich, R.J. and Wegner, G. 1987, ApJ, 313, 42
51. Ebeling, H., Voges, W., Bohringer, H., Edge, A.C., Huchra, J.P., Briel, U.G., 1996, MNRAS, 281, 799
52. Efstathiou, G., Ellis, R.S., Peterson, B.A., 1988, MNRAS, 232, 431
53. Efstathiou, G., Bridle, S.L., Lasenby, A.N., Hobson, M.P., Ellis, R.S., 1999, MNRAS, 303, L47
54. Efstathiou, G., et al, (2DFGRS TEAM), 2002, MNRAS, 330, L29 283,47
55. Einasto, J., 2001, New Astr.Rev., 45, 355
56. Eke, V.R., Cole, S., Frenk, C.S., Patrick H.J., 1998, MNRAS, 298, 1145
57. Elizalde, E., 2002, in 2^{nd} *Hellenic Cosmology Meeting*, eds. M.Plionis, S.Cotsakis, Kluwer ASSL series
58. Ettori, S., Fabian, A.C., 1999, MNRAS, 305, 834
59. Evrard A.E., Mohr J.J., Fabricant D.G., Geller M.J.,1993, ApJ, 419, L9
60. Faber, S.M., Jackson, R.E., 1976, ApJ, 204, 668
61. Freedman, W.L., et al., 2001, ApJ, 553, 47
62. Gibson, B.K. & Brook, C.B., 2001, in *New Cosmological Data and the Values of the Fundamental Parameters*, ASP Conf. Series, Vol.666, eds. A.Lasenby & A.Wilkinson
63. Gioia, I., 2001, in the proceedings *Chemical Enrichmen of Intracluster and Intergalactic Medium*, Vulcano-Sicily, *astro-ph/0107452*
64. Giovanelli, R., Dale, D.A., Haynes, M.P., Hardy, E. & Campusano, L.E., 1999, ApJ, 525, 25
65. Girardi, M. & Mezzetti, M., 2001, ApJ, 548, 79
66. Governato, F., 2002, in*Tracing Cosmic Evolution with Galaxy Clusters*, ASP Conference Series, in press, *astro-ph/0201493*
67. Hanany S., et al, 2000, ApJ, 545, L5
68. Henry, J.P., 2000, ApJ, 534, 565

69. Henry, J.P., 2002, in *High-z Clusters, Missing Baryons & CMB Polarization*, ASP Conf.Series, Vol.999, Eds. Chen L.W. et al.
70. Hoyle, F., Outram, P.J., Shanks,T., Croom, S.M., Boyle, B.J., Loaring, N.S., 2002, MNRAS, 329, 336 Miller, L.; Smith, R. J.
71. Hu, W., Sygiyama, N., Silk, J., 1997, Nature, 386, 37
72. Huchra, J., Davis, M., Latham, D., Tonry, J., ApJ Suppl., 1983, 52, 69
73. Hudson, M.J., 1993, MNRAS, 265, 72
74. Hudson, M.J.; Dekel, A., Courteau, S., Faber, S.M., Willick, J.A., 1995, MNRAS, 274, 305
75. Hudson, M.J., Smith, R.J., Lucey, J.R., Schlegel, D.J., Davies, R.L., 1999, ApJ, 512. L79
76. Jensen, J.B., et al, 2001, ApJ, 550, 503
77. Jetzer, Ph., Koch, P., Piffaretti, R., Puy, D. & Schindler, S., 2002, *astro-ph/0201412*.
78. Kaiser, N., 1987, MNRAS, 227, 1
79. Kaiser, N., 1984, ApJ, 284, L9
80. Klypin, A.A., Primack, J.R., Holtzman, J., 1996, ApJ, 466, 1
81. Kolokotronis, V., Basilakos, S., Plionis, M., Georgantopoulos, 2001, MNRAS, 320, 49
82. Kolokotronis, V., Basilakos, S., Plionis, M., 2002, MNRAS, in press
83. Koopmans, L.V. & Fassnacht, C.D., 1999, ApJ, 527, 513
84. Krauss, L.M. & Chaboyer, B., 2002, Nature, in press, *astro-ph/0111597*
85. Lacey, C., Cole, S., 1996, MNRAS, 262, 627
86. Lahav, O., Rees, M.J., Lilje, P.B., Primack, J., 1991, MNRAS, 251, 128
87. Lahav, O., 2001, in *New Cosmological Data and the Values of the Fundamental Parameters*, IAU Symposium 201
88. Lahav, O., et al., 2002, MNRAS, in press,*astro-ph/0112162*
89. Lauer, T.R., Postman, M., 1994, ApJ, 425, 418
90. Lee, A.T., et al., 2001, ApJ, 561, L1
91. Leibundgut, B., 2001, AARA, 39, 67
92. Livio, M, 2000, in *Type Ia Supernovae: Theory and Cosmology*, Cambridge Univ. Press
93. Lucey, J.R., Carter, D. 1988a, MNRAS, 231, 15p
94. Lynden-Bell, D., Faber, S.M., Burstein, D., Davies, R.L., Dressler, A., Terlevich, R.J. and Wegner, G. 1988, ApJ, 326, 19
95. Maddox, S.J., Efstathiou, G., Sutherland, W.J. & Loveday, J., 1990, MNRAS, 242, 43.
96. Maddox S.J. , Sutherland W.J., Efstathiou G., Loveday, J. 1990, MNRAS, 243, 692
97. Mason, B.S., Myers, S.T., Readhead, A.C.S., 2001, ApJ, 555, L11
98. Melchiorri, A., 2001, in *COSMO-01* meeting, Finland, *astro-ph/0201237*
99. Melchiorri, A. & Griffiths, L.M., 2001, NewAR, 45, 321
100. Melott, A.L., Chambers, S.W., Miller, C.J., 2001, ApJ, 559, L75
101. Merritt, D., 1985, ApJ, 289, 18
102. Miranda, O.D., de Araujo, J.C.N., 2002, MNRAS, in press, *astro-ph/0105328*
103. Mohr, J.J., Mathiesen, B., Evrard, A.E., 1999, ApJ, 517, 627
104. Mould, J., Aaronson, M., Huchra, J., 1980, ApJ, 238, 458
105. Mulchaey, J.S., 2000, ARAA, 38, 289
106. Munshi, D., Coles, P., Melott, A., 1999, MNRAS, 310, 892
107. Olive, K., Steigman, G., Walker, T.P., 2000, Phys.Rept., 333, 389

108. Outram, P.J., Hoyle, F., Shanks, T., Boyle, B.J., Croom, S.M., Loaring, N.S., Miller, L., Smith, R.J., 2001, MNRAS, 328, 174
109. Parodi, B.R., Saha, A., Sandage, A. & Tammann, G.A., 2000, ApJ, 540, 634
110. Peacock, J.A., West, M., 1992, MNRAS, 259, 494
111. Peacock, J.A., Dodds, S.J., 1994, MNRAS, 267, 1020
112. Peacock, J.A., 2000, *Cosmological Physics*, Cambridge Univ. Press
113. Peacock, J.A., et al, 2001, Nature, 410, 169
114. Peebles, P.J.E., 1980, *Physical Cosmology*, Princeton Univ. Press
115. Peebles, P.J.E., 1993, *Principles of Physical Cosmology*, Princeton Univ. Press
116. Peebles, P.J.E., 2001, ApJ, 557, 495
117. Percival, W.J., et al (2DFGRS TEAM), 2001, MNRAS, 327, 1297
118. Perlmutter, S., et al., (Supernova Cosmology Project), 1995, ApJ. 440, L41
119. Perlmutter, S., et al., (Supernova Cosmology Project), 1999, ApJ. 517, 565
120. Plionis M., 2001, in the proceedings of the *Clusters and the High-Redshift Universe observed in X-rays*, XXI$^{\rm th}$ Moriond Astrophysics Meeting, eds. Neumann et al.
121. Plionis, M, Barrow, J.D. & Frenk, C.S. 1991, MNRAS, 249, 662
122. Plionis, M. & Valdarnini, R. 1991 MNRAS, 249, 46
123. Plionis, M. & Kolokotronis, V., 1998, ApJ, 500, 1
124. Plionis, M., Basilakos, S., Rowan-Robinson, M., Maddox, S.J., Oliver, S.J., Keeble, O., Saunders, W., 2000, MNRAS, 313, 8
125. Plionis, M. & Basilakos, S., 2002a, MNRAS, 329, L47
126. Plionis, M. & Basilakos, S., 2002b, MNRAS, 330, 399
127. Plionis, M., 2002, ApJ, 572, L?
128. Press, W.H., Schechter, P., 1974, ApJ, 187, 425
129. Primack, J.R., 1999, in *Formation of Structure in the Universe*, Eds. Dekel & Ostriker, p.3, Camb. Univ. Press
130. Pryke, C., Halverson, N.W., Leitch, E.M., Kovac, J., Carlstrom, J.E., Holzapfel, W.L., Dragovan, M., 2002, ApJ, in press, *astro-ph/01044909*
131. Rafaeli, Y., 2002, in proceedings of the Erice NATO/ASI *Astrophysical Sources of High Energy Particles and Radiation*
132. Ramella, M., Geller, M.J. & Huchra, J.P. 1989, ApJ, 344, 522
133. Reiprich, T.H., Böhringer, H., 2002, ApJ, in press, *astro-ph/0111285*
134. Richstone, D., Loeb, A., Turner, E.L., 1992, ApJ, 393, 477
135. Riess, A.G., et al., 1998, AJ, 116, 1009
136. Riess, A.G., 2000, PASP, 112, 1284
137. Riess, A.G., et al., 2001, ApJ, 560, 49
138. Ritchie, B.W., Thomas, P.A., 2002, MNRAS, 329, 675
139. Roettiger, K., Burns, J. & Loken, C., 1993, ApJ, 407, L53
140. Roettiger, K., Stone, J.M., Burns, J., 1999, ApJ, 518, 594
141. Rood, H.J., Page, T.L., Kintner, E.C., King, I.R., 1972, ApJ, 175, 627
142. Rose, J.A., Gaba, A.E., Christiansen, W.A., Davis, D.S., Caldwell, N., Hunstead, R.W., Johnston-Hollitt, M., 2002, AJ, 123, 1216
143. Rowan-Robinson, M., 1985, *The cosmological distance ladder: Distance and time in the universe*, New York, W. H. Freeman and Co.
144. Rowan-Robinson, M., 1988, Space Science Reviews, 48
145. Rowan-Robinson, M., et al., 2000, MNRAS, 314, 375
146. Rowan-Robinson, M., 2001, in *IDM2000: 3rd International Workshop on Identification of Dark Matter*, ed. N.Spooner (World Scientific)
147. Sadat, R. & Blanchard, A., 2001, AA, 371, 19
148. Sahni, V., 2002, in proceedings of *The Early Universe and Cosmological Observations: a Critical Review*, to appear in Clas.Quant.Grav., *astro-ph/0202076*

149. Sandage, A. & Tammann, G.A., 1995, ApJ, 446, 1
150. Sarazin, C.L., 2001, in *Merging Processes in clusters of Galaxies*, eds. Feretti, L., Gioia, M., Giovannini, G., (Dordrecht: Kluwer)
151. Scaramella, R., Baiesi-Pillastrini, G., Chincarini, G., Vettolani, G. & Zamorani, G. 1989, Nature, 338, 562
152. Scaramella, R., Vettolani, G. & Zamorani, G. 1991, ApJ, 376, L1
153. Schechter, P., 1976, ApJ, 203, 297
154. Schindler S., 1999, in proceedings of the Vulcano Workshop 1999, *Multifrequency Behaviour of High Energy Cosmic Sources*, eds. Giovanelli F., Sabau-Graziati L., *astro-ph/9909042*
155. Schindler S., 2001, Space Science Reviews, ISSI, Vol.15, Eds. P.Jetzer, K.Pretzl, R.von Steiger, (eds.), Kluwer
156. Schmidt, B.P., et al., 1998, ApJ, 507, 46
157. Schuecker, P., Böhringer, H., Reiprich, T.H., Feretti, L., 2001, AA, 378, 408
158. Sigad, Y., Eldar, A., Dekel, A., Strauss, M.A., Yahil, A., 1998, ApJ, 495, 516
159. Smoot, G.F., et al, 1991, ApJ, 371, L1
160. Smoot, G.F., 2000, Phys.Rep., 333, 269
161. Sofue, Y., 1997, PASJ, 49, 17
162. Sofue, Y., Rubin, V., 2001, AARA, 39, 137
163. Steigman, G., 2001, in "*The Light Elements and Their Evolution*, IAU Symp. 198, eds L. Da Silva, M. Spite, J.R. Medeiros, ASP Conf. Series.
164. Stompor, R. et al., 2001, ApJ, 561, L7
165. Stoughton, C. et al., 2002, AJ, 123, 485
166. Strauss, M.A. & Willick, J., 1995, Phys.Rep., 261, 271
167. Struble, M.F. & Rood, H.J. 1999, ApJ Suppl., 125, 35
168. Sugiyama, N., 1995, ApJ Suupl., 100, 281
169. Sunyaev, R.A. & Zeldovich, Ya.B., 1970, A&SS, 7, 3
170. Szalay, A.S., et al. (SSDS COLLABORATION), 2002, ApJ, in press, *astro-ph/0107419*
171. Tammann, G.A., 1999, in *Recent Developments in Theoretical and Experimental General Relativity, Gravitation, and Relativistic Field Theories*, Eds T.Piran & R.Ruffini. World Scientific Publishers, p.243
172. Tegmark, M., Hamilton, A.J.S., Xu, Y., 2002, MNRAS, in press, *astro-ph/0111575*
173. Tomita, K., 2001, MNRAS, 326, 287
174. Tonry, J.L., Blakeslee, J.P., Ahjar, E.A., Dressler, A., 2000, ApJ, 530, 625
175. Tully, B. & Fisher, J.R., 1977, ApJ, 54, 661
176. Tully, R.B., Scaramella, R., Vettolani, G. Zamorani, G., 1992, ApJ, 388, 9
177. Tutui, Y., Sofue, Y., Honma, M., Ichikawa, T., Wakamatsu, K., 2001, PASJ, 53, 701
178. van den Bergh, S., 1998, *Galaxy morphology and classification*, Cambridge University Press
179. van de Weygaert, R., 2002, in 2^{nd} *Hellenic Cosmology Meeting*, eds. M.Plionis, S.Cotsakis, Kluwer ASSL series
180. Viana, P.T.P., Liddle, A.R., 1999, MNRAS, 303, 535
181. Wang, X., Tegmark, M., Zaldarriaga, M., 2002, Phys.Rev.D, in press, *astro-ph/0105091*
182. Webster, A.M., Bridle, S.L., Hobson, M.P., Lasenby, A.N., Lahav, O., Rocha, G., 1998, ApJ, 509, L65
183. Weinberg, S. 1972, *Gravitation & Cosmology*, John Wiley, New York.
184. West, M. J., 1994, MNRAS, 268, 79
185. White, D.A., 2000, MNRAS, 312, 663

186. White, S.D.M., Navarro, J.F., Evrard, A.E., Frenk, C.S., 1993, Nature, 366, 429
187. Willick, J.A., Strauss, M.A., 1998, ApJ, 507, 64
188. Willick, J.A. 1999, ApJ, 522, 647
189. Willick, J.A. 2000, in *Energy Densities in the Universe*, XXXVth Rencontres de Moriond, *astro-ph/0003232*
190. Willick, J.A., Batra, P., 2001, ApJ, 548, 564
191. Yahil, A., 1985, in Workshop on the *Virgo CLuster of Galaxies*, ed. O.G. Richter & B. Bingelli (Munich:ESO), 350
192. Zabludoff, A.I. & Zaritsky, D., 1995, ApJ, 447, L21
193. Zehavi, I., Riess, A.G., Kirshner, R.P.; Dekel, A., 1998, ApJ, 503, 483
194. Zeldovich, Ya.B., Einasto, J. & Shandarin, S.F., 1982, Nature, 300,407
195. Ziegler, B.L. et al., 2002, ApJ, 564, L69

This figure "plio3.jpg" is available in "jpg" format from:

http://lanl.arXiv.org/ps/astro-ph/0205166


This figure "plio10.jpg" is available in "jpg" format from:
http://lanl.arXiv.org/ps/astro-ph/0205166